Final Report

Project Title: Innovative Application of Maintenance-Free Phase-Change Thermal Energy Storage for Dish-Engine Solar Power Generation

Project Period: 09/30/08 – 08/30/12

Budget Period: Phase 2, 09/01/09 – 08/30/12

Budget Period Budget: $1,848,674

Submission Date: 1/23/2013

Recipient: Infinia Corporation

Address: 6811 West Okanogan Place
Kennewick, WA 99336

Award Number: DE-FC36-08GO18157

Project Team: Pennsylvania State University Applied Research Laboratory
Thermacore, Inc.

Submitted By: Songgang Qiu, Ph. D.
Vice President, Research and Development
Phone: 509-737-2119
Fax: 509-736-3660
Email: sqiu@infiniacorp.com

GO Contracting Officer: Diana Bobo

Technology Project Officer: Thomas Rueckert

DOE Technical Manager: Joseph Stekli

Executive Summary

This final report summarizes the final results of the Phase II Innovative Application of Maintenance-Free Phase-Change Thermal Energy Storage for Dish-Engine Solar Power Generation project being performed by Infinia Corporation for the U.S. Department of Energy under contract DE-FC36-08GO18157 during the project period of September 1, 2009 – August 30, 2012.

The primary objective of this project is to demonstrate the practicality of integrating thermal energy storage (TES) modules, using a suitable thermal salt phase-change material (PCM) as its medium, with a dish/Stirling engine; enabling the system to operate during cloud transients and to provide dispatchable power for 4 to 6 hours after sunset.

A laboratory prototype designed to provide 3 kW-h of net electrical output was constructed and tested at Infinia's Ogden Headquarters. In the course of the testing, it was determined that the system's heat pipe network – used to transfer incoming heat from the solar receiver to both the Stirling generator heater head and to the phase change salt – did not perform to expectations. The heat pipes had limited capacity to deliver sufficient heat energy to the generator and salt mass while in a charging mode, which was highly dependent on the orientation of the device (vertical versus horizontal). In addition, the TES system was only able to extract about 30 to 40% of the expected amount of energy from the phase change salt once it was fully molten. However, the use of heat pipes to transfer heat energy to and from a thermal energy storage medium is a key technical innovation, and the project team feels that the limitations of the current device could be greatly improved with further development.

A detailed study of manufacturing costs using the prototype TES module as a basis indicates that meeting DOE LCOE goals with this hardware requires significant efforts. Improvement can be made by implementing aggressive cost-down initiatives in design and materials, improving system performance by boosting efficiencies, and by refining cost estimates with vendor quotes in lieu of mass-based approaches.

Although the prototype did not fully demonstrate performance and realize projected cost targets, the project team believes that these challenges can be overcome. The test data showed that the performance can be significantly improved by refining the heat pipe designs. However, the project objective for phase 3 is to design and test on sun the field ready systems, the project team feels that is necessary to further refine the prototype heat pipe design in the current prototype TES system before move on to field test units, Phase 3 continuation will not be pursued.

Table of Contents

Background

The current state-of-the-art for the application of TES to solar dish systems is virtually non-existent. Solar TES is most often associated with trough and central receiver systems. Trough TES systems include several candidate approaches with widely varying stages of development. The LUZ SEGS I trough, using the primary mineral oil heat transfer fluid (HTF) in hot and warm tanks, provided 3 hours of daily direct energy storage capacity between 1985 and 1999. The 10-MW Solar 2 central receiver system demonstrated the viability of molten salt TES in the late 1990’s. These and most other direct and indirect solar TES systems use sensible heat capacity stored in the liquid state, are relatively inefficient with typical solar-to-electric efficiencies of 15 to 20%, require complex pumping systems, and typically require large installations with plant sizes in the 10’s or 100’s of MW to be economically viable. These molten salt systems must avoid salt freezing. The entire system may be shut down with any freezing or when a component within the TES requires maintenance or fails. Phase change materials (PCMs), which provide a large increase in energy storage density by utilizing the latent heat of fusion, are typically used only for low-temperature storage in space heating and water heating applications. The Infinia approach is an innovative implementation of a PCM that is closely integrated with the engine and solar receiver. As with the Infinia FPSE, the TES module is hermetically sealed and maintenance-free. It is a passive heat transport system that requires no insulated pumps, fittings or other components to transport hot fluid, and is unaffected by ambient temperature levels or melt-freeze cycles. It is also distributed, so any problem that develops will only impact a single engine.

Introduction

An often sought-after feature of solar power is to provide electricity in a dispatchable manner during cloud transient and non-daylight hours. Infinia's concept is to incorporate a TES module that contains a thermal salt phase-change material (PCM) between the solar thermal receiver and the engine. Concentrated solar flux will enter the receiver and be conducted into the PCM by heat pipes. The salt will undergo melt-freeze cycles near Infinia's optimal engine operating temperature in the 600°C to 700°C range, harnessing the latent heat storage of the salt and avoiding any complicated pumped loops or freezing/maintenance issues. Heat will also be conducted from the PCM to the engine heater head via heat pipes. In this phase, the solar TES module is designed to provide sufficient storage for 1 hour of operation at an average power output of 3 kW_e and is expected to support the DOE 2020 levelized cost of energy (LCOE) goal of 5¢/kWh, adjusted for the real cost of conventional fuels, and to offer a round trip efficiency of at least 93% for a net cost below \$15/kW-h_T in volume production.

The inclusion of a heat-pipe-based TES component at the engine pod of a dish-Stirling system has the potential for many positive performance impacts. Each individual unit will see an increased energy output as the dish can be oversized to allow daytime collection of thermal energy for use during nighttime or cloudy periods, reducing the overall LCOE of the system by increasing runtime. A PCM TES solution located at the engine pod will have no pumped loops and will not experience the same maintenance issues associated with other centralized trough and power tower TES systems. No fluids are being pumped so there are no issues with high-temperature pumps or frozen loops that can take an entire field out of operation. Should a problem occur, only one 3-kW system in a large array will experience issues, allowing the majority to remain in operation. Probably the largest impact will be in lower capital costs for the CSP system in general. Infinia's experience in developing its PowerDish™ product has shown that maintaining optical accuracy for an acceptable heat flux profile at the heater head of the Stirling engine is costly. By using a TES/heat pipe concept, the heater head and solar receiver are decoupled, allowing for much more variability of the solar flux at the receiver. The TES and heat pipes deliver heat to the engine uniformly. This lowers the optical accuracy required by the concentrator reducing costs in the concentrator, the chassis/stand, the tracking drive, the heater head components and a variety of other subsystems. Efficiency is increased because the heater head will be uniformly heated, so it can be operated at a higher average hot end temperature without developing hot spots that exceed materials limitations.

Utilization of the latent heat of fusion in a PCM TES device greatly improves the specific weight and volume relative to single-phase TES systems and enables the practical use of an integrated receiver/TES/engine module. There are many pure and eutectic salts, mostly alkali halides, with attractive properties to provide the TES function. For the Infinia 3-kW Stirling engine interface, it is advantageous to select a salt with a melting point in the 600 to 700°C range so that the extended operation during phase change is near the peak system efficiency. In Phase 1, Infinia chose the eutectic NaF/NaCl. Pure NaF melts at 993°C and pure NaCl melts at 801°C. As the salts are mixed, the melting point is depressed, reaching a minimum of 680°C at the eutectic point of 34 Mol% NaF and 66 Mol% NaCl. This permits extended operation using the latent heat of fusion at the eutectic melt temperature. A comparable amount of energy from both liquid and solid sensible heat capacity can also be extracted by operating over a wide temperature range, from about 750 down to 400°C. The conversion efficiency of the Stirling cycle will decrease as the temperature drops, but the 3-kW engine will continue to generate useful kW-h of energy down to the lower temperature bound.

In Phase 1, the Infinia team conducted trade studies and developed a preliminary design for the TES/CSP system prototype to be built and tested in Phase 2. Once the preliminary design was finished, the Phase 2 Tasks were completed as summarized below. It should be noted that Tasks 4 and 5 were added to the Statement of Project Objectives (SOPO) after the original TES module failed during testing.

Task 1: Detailed Integrated Design - Based on the results of the Phase 1 preliminary design, this task developed the detailed drawings, bill of materials (BOM) and technical specifications necessary to procure or manufacture and to assemble all component parts and subassemblies of the system. Subcontractor Thermacore finalized the detailed TES design, drawing on vast experience with high temperature heat pipes to insure manufacturability and reliability.

Task 2: Fabricate, Integrate TES/CSP Prototype – In this phase, all component parts of the prototype demonstration system are purchased or fabricated. Parts common to the PowerDish™ are procured from the commercial supply chain. New and modified parts will be fabricated in the on-site Infinia machine shop where practical, with Thermacore and other established vendors utilized for specialty items where appropriate. All subsystems will be assembled and checked out independently where practical, prior to final integration into the complete prototype demonstration system.

Task 3: Increased Dish Capacity Design - The existing Infinia solar dish is sized for real time direct heating of the engine. For the utilization of this dish with the TES prototype in Phase 2, it will be necessary to operate with the engine at part load during some of the day in order to divert some of the available solar input for heating the salt. A more desirable operating mode is to increase the thermal capacity of the dish so that the necessary heat storage in the salt can be provided while operating the engine at full output for the day. In Task 3, specific target operating scenarios were evaluated and the preferred new dish size selected. The design for the new dish, including all structural elements, is established.

Task 4: Evaluate TES Module Repair - Assess the damage incurred during the breach of the TES module and determine how to avoid another breach through lessons learned from the failure analysis. A refinement of the earlier structural analyses using FEA was completed to assess whether a new receiver design is required.

Task 4 Go/No Go Criteria This task to be completed by 2/15/2012 and a report detailing any findings and design changes will be delivered to DOE.

Task 5: Repair TES Module - Based upon information gathered in Task 4, the TES module will be repaired with any necessary incorporation of design changes to avoid the recurrence of the TES module breach.

Task 5 Go/No Go Criteria This task to be completed by 4/30/2012 and a report detailing the completion of the repair and any further design refinements or performance concerns due to the use of a refurbished container will be delivered to DOE.

Task 6: Test and Evaluate TES/CSP System Prototype - An engine test cell is established, including all necessary instrumentation. A LabView™-based data acquisition system was acquired and established LabView™ VI’s were adapted to address the special requirements of the prototype. The primary test goal is to fully characterize the operational characteristics of the TES and to map performance of the TES over a wide range of operating and environmental conditions.

Task 7: LCOE Refinement – The cost analysis that was conducted in Phase 1 was revisited, including changes in cost elements and updated O&M cost projections. Reasons for change include such items as feedback from vendors during TES production; TES design changes to improve performance or cost, new production candidates identified, and development of or identification of improved or lower cost processing.

Task 8: - Project Management and Reporting - Project Management will occur as a task in each phase. The task will coordinate overall efforts and capture the work related to reporting, presentations and ensuring project goals are met. Specific items derived from this task will include a Final Report containing technical and evaluation results of the prototype, and a revised production cost analysis (LCOE). Quarterly reports, annual reports, and annual presentations will also be produced.

Overall Phase 2 Go/No Go Criteria - Based on results of the Phase 2 design, cost analysis and prototype demonstration results presented in the Phase 2 reports and presentations, DOE can assess project progress and viability for consistency with meeting both performance and 2015 and 2020 CSP/TES system goals of LCOE comparable to intermediate power (7

¢/kW-h) by 2015 and baseload power (5 ¢/kW-h) by 2020, adjusted based on the real costs for conventional fuels.

Project Results and Discussion

Task 1: Detailed Integrated Design

Broadly speaking, the detailed design of the 1-hour TES/engine system prototype included three sub-categories: the dish and supporting structures (PowerDish™ modifications), the TES/engine module itself, and the laboratory test stand in which the TES module is tested prior to on-sun testing with the dish.

Although it is desirable to supply the TES module with more thermal energy than the engine can consume such that excess will be absorbed by the PCM, budgetary constraints precluded fabricating a dish larger than the standard PowerDish™. Therefore, a standard 14.8m^2 concentrator was modified for use in this project (Figure 1); the details of which are discussed in the following.

Concentrator Boom Arms/Chassis - The boom arms attach to the dish chassis and support the engine/TES module, as well as the balance of plant items, collectively called the Heat Drive. These arms were redesigned to move the heat drive away from the dish to compensate for the added length of the TES module, thereby maintaining proper focal length. Finite Element Analysis (FEA) methods were used to ensure that the material stresses are within allowable limits at the extremes of the heat drive tracking positions.

TES Support – The TES module weighs approximately 165 lb (PCM and structure), and is welded to a ring that has been brazed to the Stirling engine heater head. The support was designed using an approach similar to the engine suspension used in the PowerDishTM, namely, flexure supports that are compliant in the axial direction (out-of-plane) to allow for vibration and thermal expansion, while providing high in-plane stiffness to support the added weight of the TES module.

TES Module - The prototype TES subsystem is shown in Figure 2 below for reference. The subsystem is composed of a 3 kW Stirling engine; whose heater head serves as the condenser section of the central heat pipe, a salt storage container; which holds the mass of NaF/NaCl eutectic phase change material into which the input (secondary) heat pipes are embedded, receiver vapor chamber; which makes up the evaporator section of the central (primary) heat pipe, supporting flexures for both the engine and TES module, and the support frames to which the supporting flexures are mounted.
A comprehensive design review of the TES module was conducted at Thermacore headquarters in Lancaster, PA prior to the start of construction. Topics discussed were the results of the thermal and structural analyses, wick selection, fabrication and processing sequence, and safety.

Figure 1, PowerDish^{TM} Concentrator Modified for TES

Wick analysis and selection are important considerations for finalizing the TES module design. The heat transfer limits for the heat pipes were examined in light of the required capacities versus operating temperatures. These limits are mainly the capillary limit and sonic limit. During daytime operation/charging, concentrated solar energy impinges on the receiver surface. The nominal heating rate supplied by the concentrator dish is 12kW distributed over a 30cm diameter evaporator.

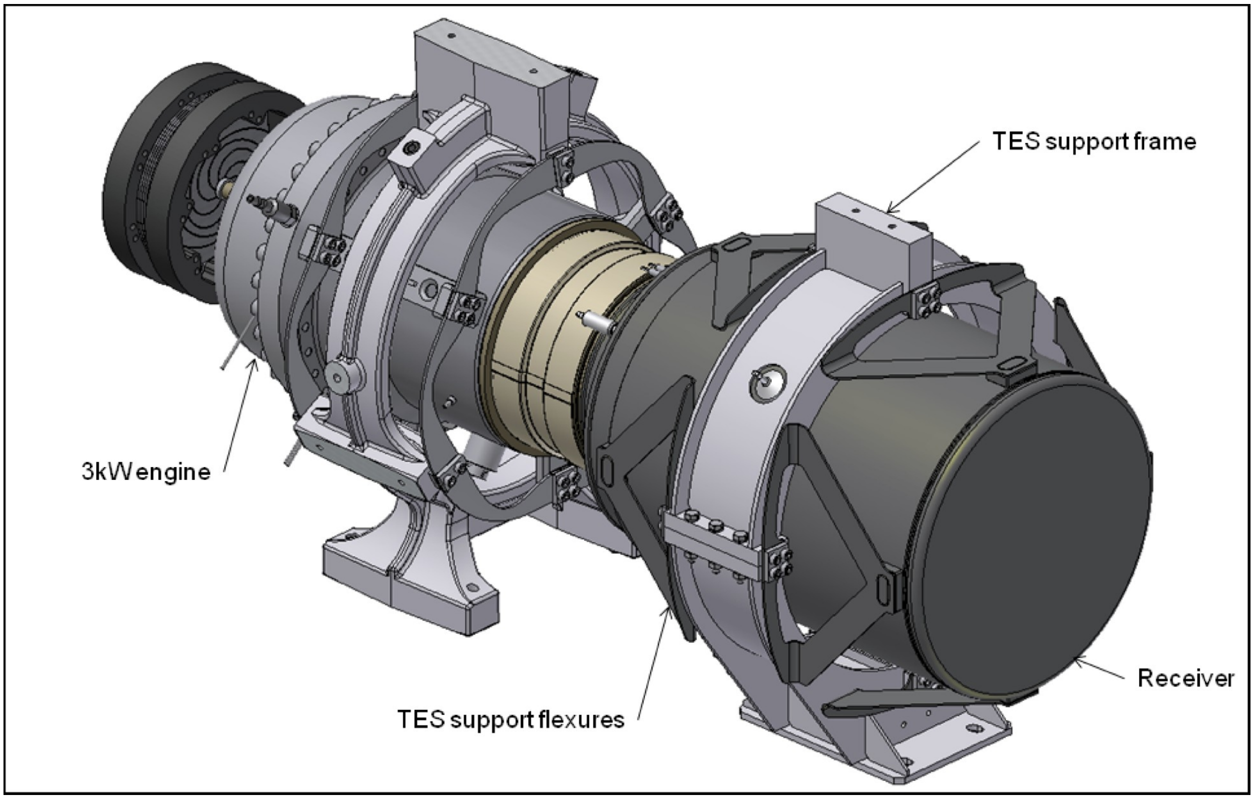

Figure 2, Stirling Generator/TES Module Sub-Assembly

The engine heater head, as well as a total of 32 0.5” diameter heat pipes embedded in the NaF/NaCl salt serve as the condenser. Although the engine can accept the full 12kW heat input via the primary heat pipe, the engine will be run at part load – perhaps 10kW input – in order that the balance of the heat energy will be transferred to the salt via the secondary heat pipes. Three cases are examined in the wick analysis:

1. Charging – gravity neutral (sunrise, sunset, TES module horizontal)
2. Charging – gravity aided for primary heat pipe, adverse for secondary heat pipes (mid-day, TES module vertical and receiver down)
3. Discharging – gravity aided for secondary heat pipes (TES module vertical, receiver down)

An analysis of the first case (gravity neutral) showed adequate capillary pressure for condensate return in both the primary and secondary heat pipes. In the second case (vertical), the orientation of the TES module allows condensate to return to the evaporator by gravity via the primary heat pipe; no wicking is required. However, condensed liquid in the secondary heat pipes must travel the length of the heat pipes against gravity in order to reach the primary heat pipe, and finally the evaporator. Thermacore employed a proprietary FEM analysis for the wick capillary pressure field. Of a required maximum capillary pressure of 2140 Pa, the FEM results predict 3100 Pa available from the selected wick. In the third and final case, the array of secondary heat pipes now serves as the evaporator section of the device. During TES discharge, the tracking drive will be used to orient the heat drive vertically; similar to that of mid-day. In this orientation, condensate can return to the heat pipes via gravity and wicking is not required.

Infinia conducted the structural analysis of the TES vessel itself. The primary concern in this regard is the case where the system first starts up, say in the morning. At system start up, the entire TES structure as well as the PCM salt within it is at room temperature, or “cold”. The receiver, when brought on-sun, will very quickly become hot, and start to expand causing thermal stress to develop because of the adjacent structures in contact with the cold salt. Stress analysis using finite element methods provide a basis for designing a control algorithm to modulate the heating rate at the receiver such that material limits are not exceeded. Thermocouples strategically placed on the surface of the TES module such that real-time temperatures of the structure can be monitored are used in the control scheme.

FEA models were used to simulate thermal loading of the TES vessel in order to determine the effect of heating rates on the structure. Transient analyses were performed, and the data collected were the temperatures at selected probe locations as well as resultant stress, in addition to the maxima in the entire model over the entire time range. These values were plotted in order to observe trending.

After studying the results of the data, an approach was developed for cold start-up whereby heat input is ramped up while limiting the temperature gradient at the receiver as measured by appropriate thermocouple measurements.

Task 2: Fabricate/Integrate TES/CSP Prototype

Infinia developed a procedure to braze a weld ring to the heater head manifold in order to provide a point of attachment for the TES module as well as form a portion of the heat pipe vapor chamber surrounding the heater head. This modified heater head, cold heat exchanger and engine housing are laser welded to form the so-called “forward boundary”, which was sent to Thermacore for attachment of the TES module.

After welding the forward boundary to the TES module, the device is ready for salt and sodium filling. The sodium space is processed first. To prepare for filling, the TES module is subjected to a high-temperature vacuum bake-out to remove moisture, oxygen and other impurities from the TES interior. Once the bake-out is finished, the sodium charge is introduced into the heat pipe working fluid space, and the fill port tube is crimped and seal welded.

The next step is to fill the salt vessel. The constituent powders are combined in the proper proportion ahead of time and stored in an air-tight container. The eutectic salt mixture is poured into the vessel until full. The TES module is again baked-out under vacuum at high temperature to both melt the salt and extract moisture and impurities from it. Once the salt cools and solidifies, more salt mixture can be added to the resultant void space. This process is repeated three times before the target salt charge is achieved. Once the final bake-out is complete, the salt vessel fill tube is crimped and seal welded in a similar fashion as the sodium heat pipe side. Figure 3 shows the fully completed TES module, ready for final engine assembly at Infinia.

Once final engine assembly was completed, the TES module/engine was installed onto a test stand for system testing in a laboratory setting. This lab test used an induction heater to simulate concentrated solar energy. This lab heater used inductive coupling between a flat copper coil and the TES receiver.

Task 3: Increased Dish Capacity Design

Optical Analyses - Consulting engineers Schlaich Bergermann und Partner (SBP) completed optical analyses of a parabolic contour for both a 1-hour and 4 to 6-hour storage dish/Stirling CSP system.

For the 1-hour variant, Infinia directed SBP to create a contour for a dish with 20% larger area than the current PowerDish™.

The parabola contour is optimized by manually designing an ideal flux distribution—flat with sharp corners at the edge transition—that would occur at the receiver if the mirror surface were perfect, and the sunlight was a source of perfectly parallel light. Then, variations of sun shape (Kuiper) and mirror slope errors (1 milliradian max. in a Gaussian normal distribution) are incorporated into the contour model, and ray tracing is done to calculate the altered flux distribution. The process is iterated as required to optimize the contour. The contour chosen by SBP as one of the best is summarized in Figure 4.

Referring to the summary, the total power on the receiver is reported to be 15.33 kW. However, an actual dish will have less power. This is due to the shape of the mirrored panels; there is less actual area than represented by the theoretical panel segment. Also there is a gap in the panels where the post is located, further reducing net area. Finally, there is a consideration for shading from the boom arms. The result is an estimated 10% reduction in performance, or net power at the receiver of 13.80 kW.

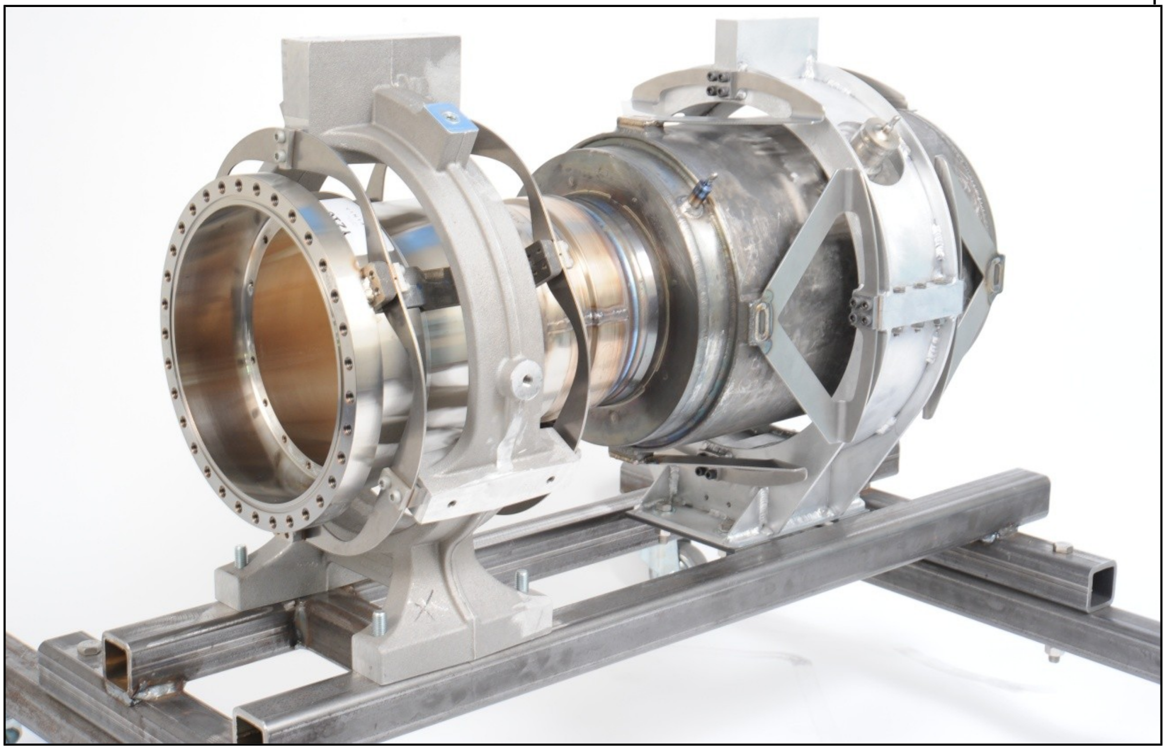

Figure 3, TES Module and Forward Boundary; Salt and Sodium Fill Completed

RESULTS:
Power on Target: 16.34 kW — Target intercept: 99.79 %
Power on Receiver: 15.33 kW — Receiver intercept: 93.62 %
Power on center hole: 0.00 kW — Center hole intercept: 0.00 %
Power on outer area: 1.02 kW — Outer area intercept: 6.22 %
receiver area: 506.71 cm^2
average flux on Receiver: 30.26 W/cm^2
Max. Flux=35.6880 W/cm^2
Max. Grad= 8.9048 $W/cm^2/cm$
(at black point on white line)
projected mirror area: 20.2830 m²
reflected power: 16.38 kW

Figure 4, 20% Larger Dish Contour Optimization Summary

For the 4 to 6-hour variant, Infinia directed SBP to create a contour for a dish with 100% larger area than the current PowerDish™. The intercept minima and flux maxima are the same as for the 1-hour variant, as well as the optimization methods. The contour chosen by SBP as one of the best is summarized in Figure 5.

As before, we can assume a net power rating of ~10% lower than the theoretical value due to geometrical constraints. Thus, the power available to the system would be 21.69 kW.

RESULTS:
Power on Target: 27.29 kW — Target intercept: 100.00 %
Power on Receiver: 24.10 kW — Receiver intercept: 88.30 %
Power on center hole: 0.00 kW — Center hole intercept: 0.01 %
Power on outer area: 3.21 kW — Outer area intercept: 11.76 %
receiver area: 506.71 cm^2
average flux on Receiver: 47.55 W/cm^2
Max. Flux=54.8089 W/cm^2
Max. Grad=11.0084 $W/cm^2/cm$
(at black point on white line)
projected mirror area: 33.7960 m^2
reflected power: 27.29 kW

Figure 5, 100% Larger Dish Contour Optimization Summary

Structural Design – The addition of 20% concentrator mirror area was judged to require only relatively minor design changes to the mirror panels themselves, with the supporting structure remaining unchanged from the current design. However, the 100% increase in mirror area required a complete re-design. Infinia again used the expertise of SBP to conduct the preliminary design of the large capacity concentrator. The results of the design effort are reviewed in the following discussion.

The first step entailed a down-select between scaling up Infinia's current PowerDish™ concentrator, and using a slumped glass reflector design that has the dish pivot in front of the support post. The latter concept does not include a slot in the concentrator for clearance around the post in stow mode, and uses a linear actuator-based elevation drive with concrete counter weight instead of the PowerDish™-style biaxial tracking drive.

A closed-dish structure is inherently much more rigid than those featuring a slot. Thus, this option likely offers cost reductions by having better utilization of materials to support the heavy thermal energy storage mass. Field alignment of the mirrors is preferred as opposed to the design approach of using high-precision, expensive components to achieve required optical accuracy. For these reasons, a scaled-up version of the PowerDish will not be pursued.

The result of the design effort is a 7.1m diameter dish, as shown in Figure 6 and Figure 7 below. Unlike the PowerDish™, the concentrator stow position is at the 0° elevation (pointed at the horizon). This allows the elimination of the slot in the dish, needed for clearance of the post for a downward stow position. The resulting structure has a closed form, and thus superior stiffness with less structure.

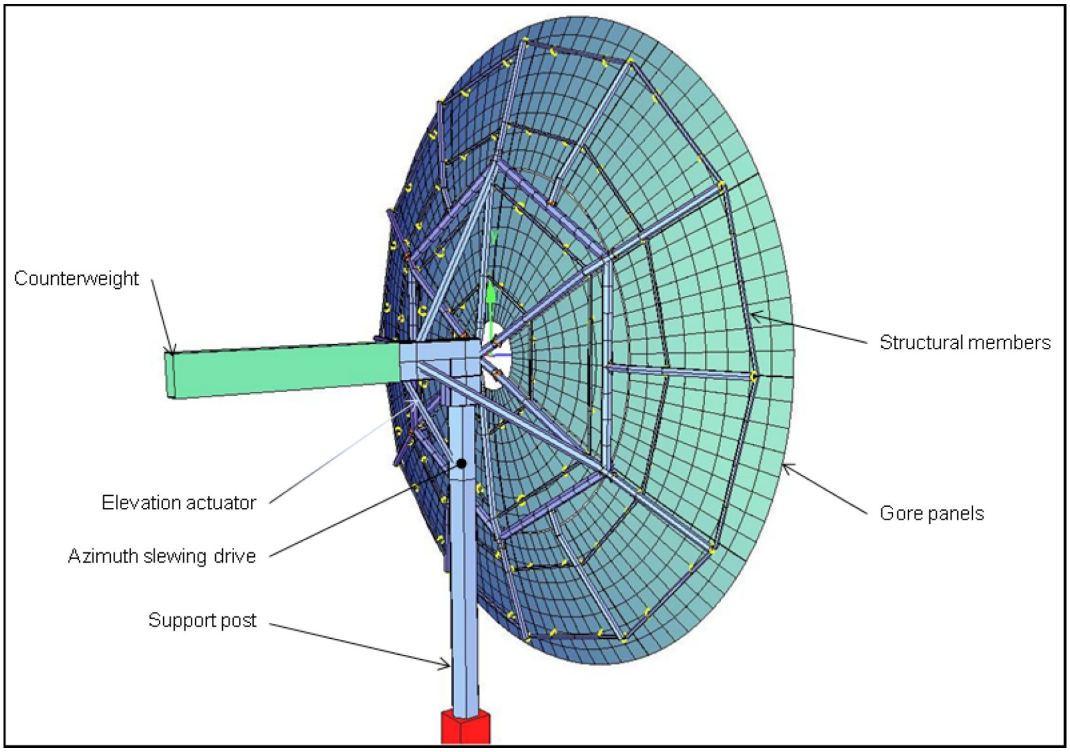

Figure 6, Increased Capacity Dish Model; Rear View

In lieu of a bi-axial tracking drive as used by the PowerDish^{TM}, the concept features a single axis slewing drive for azimuth rotation, and a linear actuator for elevation positioning. The concentrator chassis is counterweighted with a concrete beam structure to reduce loads on the elevation actuator.

Slumped glass facets are located in two rows around the optical axis. The inner row has 6, and the outer row 12 members. The mirrors have a thickness of 5 mm with a gap of 15 mm between them. Each facet has 4 support points where it is fixed to the concentrator structure. The facet angles are 60° and 30°. The facet inner and outer radii are 0.375, 1.975 and 3.55 m.

The dish structure is analyzed using the simplified finite element model. Forces from dead load and wind load are calculated. Design verification is done for all beam elements including design stress, local buckling, and global buckling. A separate stress analysis was conducted for the hub.

The utilization level (defined as actual stress divided by allowable stress) of the structural elements was kept to a maximum of about 0.5. The level is kept low for the following reasons:

- The wind tunnel data do not match exactly with the dimensions of the dish.
- The optical performance is estimated only from concentrator surface deformation.

- The chosen profiles are common hot-rolled sections with relatively thick walls.

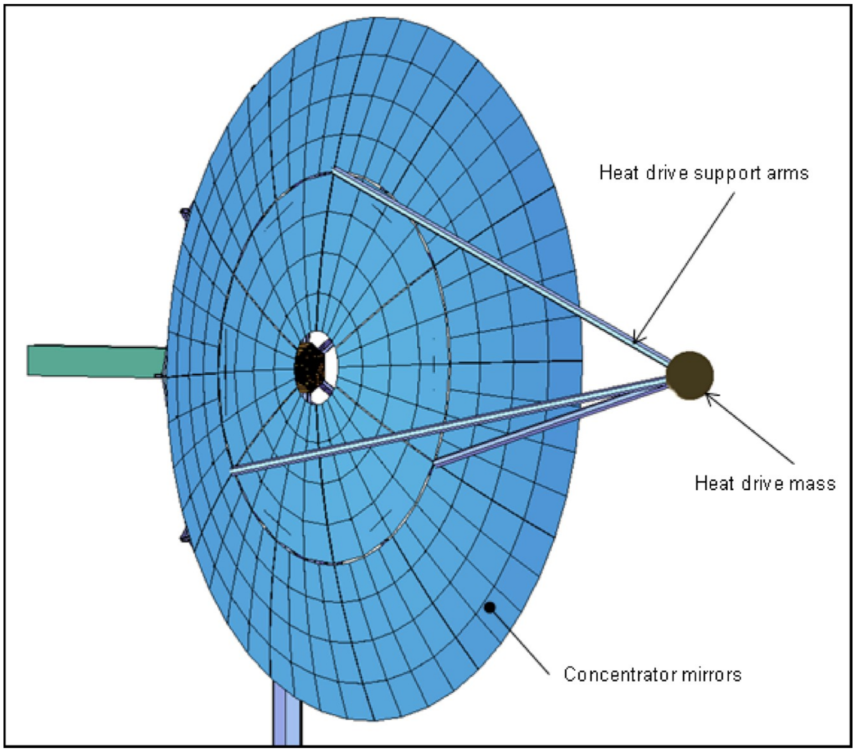

Figure 7, Increased Capacity Dish Model; Front View

Due to limited resources of time and budget, the optical performance of the dish system could not be analyzed in great detail. Instead of conducting ray-tracing analyses, the deformation of the concentrator structure at the mirror surface attachment is evaluated. The evaluation is done for one load case: dead load and wind of 10 m/s with the concentrator at the zenith (90°) position. This case combines high deformation of the structure - moment from the dead load and wind in the same direction – with a high solar radiation during mid-day. The deformation is represented by node rotations on the concentrator surface.

To make a rough estimation of the optical performance of the dish, the RMS value of the rotations is determined. For this, every facet is divided into 256 sub facets. Based on experience from previous concentrator design efforts, a target value of 1.5 mrad was defined. The results of the analysis yielded a range from 0.38 to 1.34 mrad.

Task 4: Evaluate TES Module Repair

In the summer of 2011, initial lab testing of the TES module was conducted. However, two separate test stand incidents resulted in structural failure of the TES module’s receiver plate. A failure investigation was completed to determine the root cause of the issue, the results of which are detailed in Task 6.

The purpose of this Task, which was added to the SOPO, is to evaluate the extent of the damage incurred by the TES module as a result of the receiver breach, refine the thermal/structural analysis of the receiver plate through FEA to assess whether a re-design of this component is required, and finally to determine what – if any – charge of non-condensable gas (NCG) is suitable going forward. The results of the activities described above were a guide the path forward in the repair of the TES module and subsequent testing methods.

Damage Evaluation - The first step in effecting a repair was to assess the post-failure condition of the TES module. This assessment occurred somewhat in parallel to the root cause failure analysis, as the nature and extent of the damage informs the conclusions that can be drawn.

An extensive analysis of the receiver plate itself was conducted to help determine the failure mechanism. This analysis included optical and scanning electron microscopy techniques, the results of which can be found in later in this Report. Secondary to this effort, an examination of the TES module's remaining structure and wicks was conducted. The TES module structure was visually examined for cracks and deformation which would be indicative of an over-stress condition. None were found.

Overall, there was no significant damage found throughout the TES module over and above that which was incurred in the receiver. Prior to re-attaching the receiver plate, the screen wicks within the receiver heat pipe vapor chamber were replaced.

Thermal/Structural Analysis - Previous analyses of the TES module were focused on the start-up transient response of heat input. A start-up protocol was developed to gradually ramp-up the heat into the module in order to avoid excessive thermal stresses. As a result of the receiver failure, it was decided to refine the heat input analysis to more closely model the incident flux profile that can be expected from the laboratory test stand apparatus.

Part of the root cause failure analysis effort entailed an FEA study of the heat flux incident on the receiver from the induction coil. The induction heater supplier was able to supply a flux profile based on magnetic field simulations; the heat flux as a function of radial distance is shown in Figure 8. It is important to note that this flux profile assumes an air gap of 3mm between the receiver plane and induction coil surface. The flux peaks correspond to the induction coils as shown by the dashed lines. This flux profile was applied to the TES module receiver in a steady-state analysis.

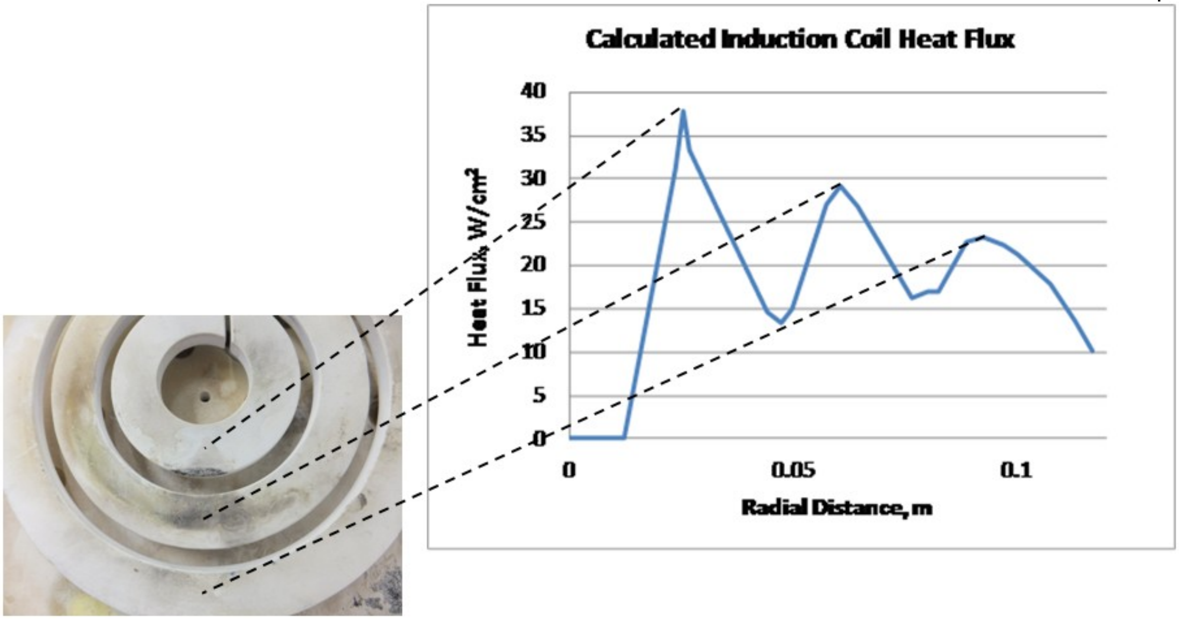

Figure 8, Induction Coil Heat Flux Profile

The resulting maximum stress in the receiver plate is approximately 140 MPa. The yield strength of Haynes 230 at 973K is approximately 200 MPa. Therefore, using a yield stress criterion for design, the receiver plate is suitable for use in its current configuration.

Although the analysis indicates that the receiver stress falls within acceptable limits, an alternative heating approach was implemented. This is because of thermal expansion. The module has the potential to grow up to 4-5mm in the axial direction at its maximum working temperature of 750°C. Since the induction coil is stationary, the air gap diminishes with higher temperature. Inductive coupling increases roughly as the inverse square of the air gap; this is likely the root cause of the failure. To address this problem, it was decided to use susceptor-based heating to conduct laboratory testing in the future. This entails heating an intermediate structure with the induction coil to a very high temperature, and in turn heating the target via radiation from that intermediary. The induction coil is used to heat silicon carbide rings to a maximum of 1500°C, while the TES is suspended above the rings to accept the radiant heat. This has the advantage of being tolerant of thermal expansion, as the heating is no longer reliant on the spacing of the target and coil. This method of heating also has a more uniform heat flux distribution. One disadvantage is reduced overall efficiency, which will result in lower total heat throughput. To further monitor critical temperatures, thermocouples are placed directly onto the receiver surface. A cross section of the susceptor test stand set-up is shown in Figure 9.

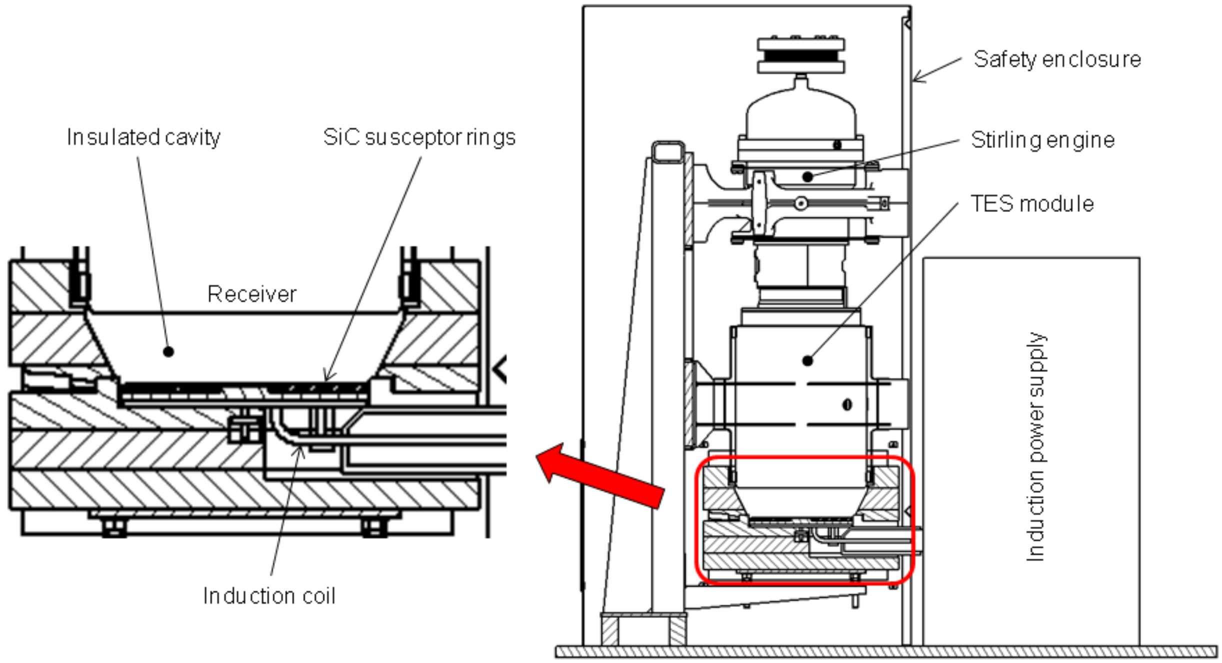

Figure 9, TES Susceptor Arrangement

Task 5: Repair TES Module

The damaged receiver plate was removed by fixturing the TES module in a mill and cutting around the perimeter at the weld where the plate joins the receiver vapor chamber diaphragm. The screen and bridge wicks were then removed and replaced. These structures are simply spot-welded in place, and can be separated from the TES assembly with relative ease.

In parallel to the receiver heat pipe vapor chamber wick replacement is the fabrication of a new receiver plate. The receiver is machined from a plate of Haynes 230, and then the back (heat pipe side) is electroless nickel plated in preparation for the nickel powder sintering. The nickel plate layer provides a surface to which the nickel powder beads can bond. The new receiver was then welded to the TES module vapor chamber diaphragm.

The next step in the repair is to perform a high-temperature vacuum bake-out of the TES module. This step ensures that moisture, oxygen and other contaminants are driven out of the heat pipe working fluid space. The heat pipe fill tube is fitted with a bellows valve, which is connected in turn to a vacuum line. The TES module is then wrapped with bead heaters.

After a week of bake-out at 750°C, the vacuum level remained constant at around 10×10^{-3} torr. The TES module was next charged with about 0.5 kg of sodium in the heat pipe space. The final heat pipe processing step is then to again heat the TES module to 750°C, and “burp” off any final residual gases under vacuum. After this last processing step, the suspension flexures were re-attached, and the device was shipped to Infinia.

Task 6: Test and Evaluate TES/CSP System Prototype

A plan outlining the procedure for testing the functionality of the TES as a stand-alone device, and then the TES/engine system as a whole has been written. In short, the first testing conducted will be to simply determine the step-wise heating rate that can be applied to the TES receiver while staying within the temperature gradient parameters appropriate to the FEA analysis described earlier. In order to decouple the engine from the TES during this phase of testing, the engine will not be charged with its helium working fluid. Then the TES/engine system will be tested by charging the salt while keeping the engine de-activated, cutting power to the heater(s), and then running the engine from the heat energy stored in the salt. During this phase of testing, it will be verified that the engine is able to extract heat from the salt and that the engine performance and run-time objectives are met. As time permits, the engine will also be run at part load while simultaneously charging the salt volume.

Prior to on-sun testing, the engine/TES module is characterized in a lab setting. Heat is supplied using an induction heater and a modified version of the solar engine test stand.

Testing of the TES module occurs in two phases. In Phase 1, the TES is charged (heated), and allowed to cool without the presence of the Stirling engine. To accomplish this, the engine housing is left empty of the displacer and convertor assemblies. The close-out cap is attached, and the engine volume is evacuated and back-filled with helium. These steps are taken to ensure that the regenerator is protected from corrosion at elevated temperatures. The TES is then heated according to a specific protocol devised to avoid excessive thermal stresses during a cold-start. In short, a difference in temperature as measured between specific locations on the TES module is monitored and kept under a certain threshold by changing the induction heater temperature set point. The temperature difference value, as well as the physical location of the measurements was derived from FEA thermal studies conducted earlier in the program.

After several charge/discharge cycles of the TES are conducted without an engine, Phase 2 testing can begin. In this phase, the engine internal assemblies are put in place, and the TES is heated according to the profiles developed in Phase 1. Here, the engine is run in parallel with charging of the TES, and electrical power is generated. After system characterization, the TES/engine assembly is ready for on-sun testing.

Test #1 - The TES module is instrumented with 24 type K thermocouples on its exterior according to the drawing in Figure 10 below.

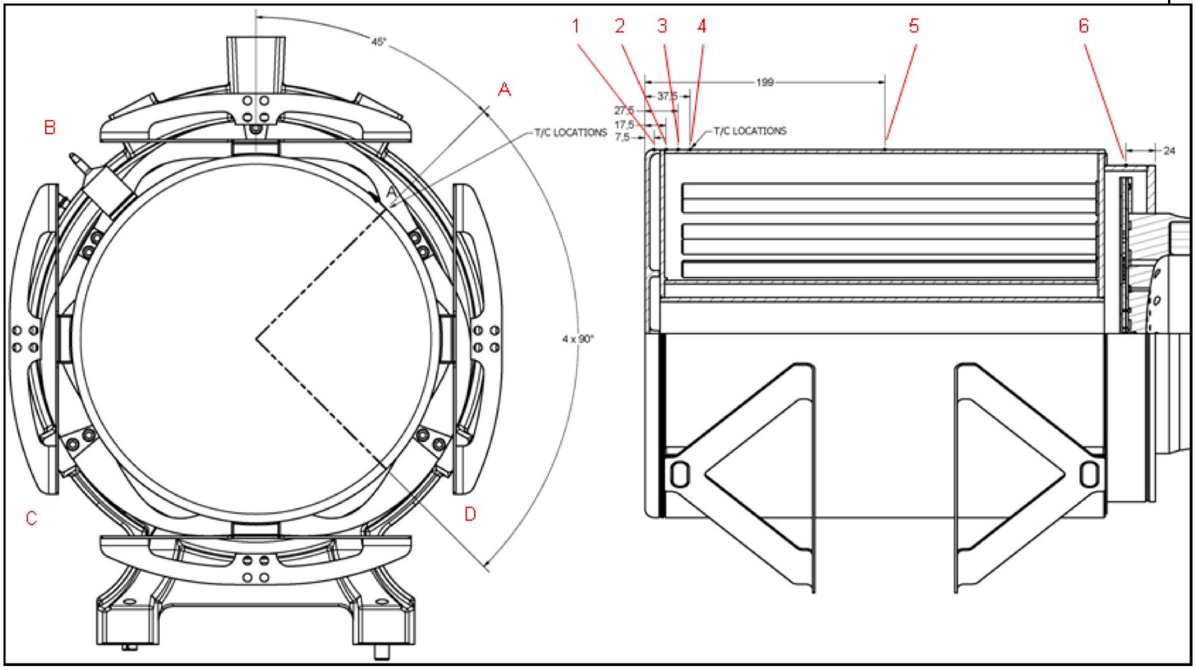

Figure 10, TES Module Thermocouple Locations

There are thermocouples located axially along the module, labeled as 1 through 6 above. These 6 positions are repeated in 4 radial locations labeled A through D. Thus, the nomenclature for the array of thermocouples is A1, A2…A6; B1, B2…B6; and so on. The purpose of the thermocouples in axial positions 1 through 4 is to get an indication of the temperature gradient from the receiver heat pipe vapor chamber, across the vapor chamber diaphragm, and into the salt vessel region. Thermocouple location 5 is located at the mid-plane between the receiver and the engine, and will give indication of the temperature of the salt mass inside the TES module. Indeed, when this thermocouple in every radial location reaches approximately 750°C, it is assured that the TES salt is completely molten. The final axial position at location 6 indicates the temperature of the heater head vapor chamber.

According to the FEA studies conducted earlier, the temperature difference between thermocouples 1 and 4 (at any radial location) should be kept below 100°C. This conservative value is meant to prevent large temperature gradients, and therefore thermal stresses, in the TES structure. During heating, the temperature set point of the induction heater is gradually raised, keeping the temperature difference below this threshold. The induction heater control thermocouple is located at axial position 1; closest to the receiver surface being heated. Also of interest is the temperature difference between locations 1 and 6. A properly functioning heat pipe is nearly isothermal along its length, so the difference should be small. It should be noted however, that due to heat pipe limitations such as the sonic limit, this last statement is only true once the heat pipe reaches its effective operating temperature. In this case, this occurs at approximately 600°C.

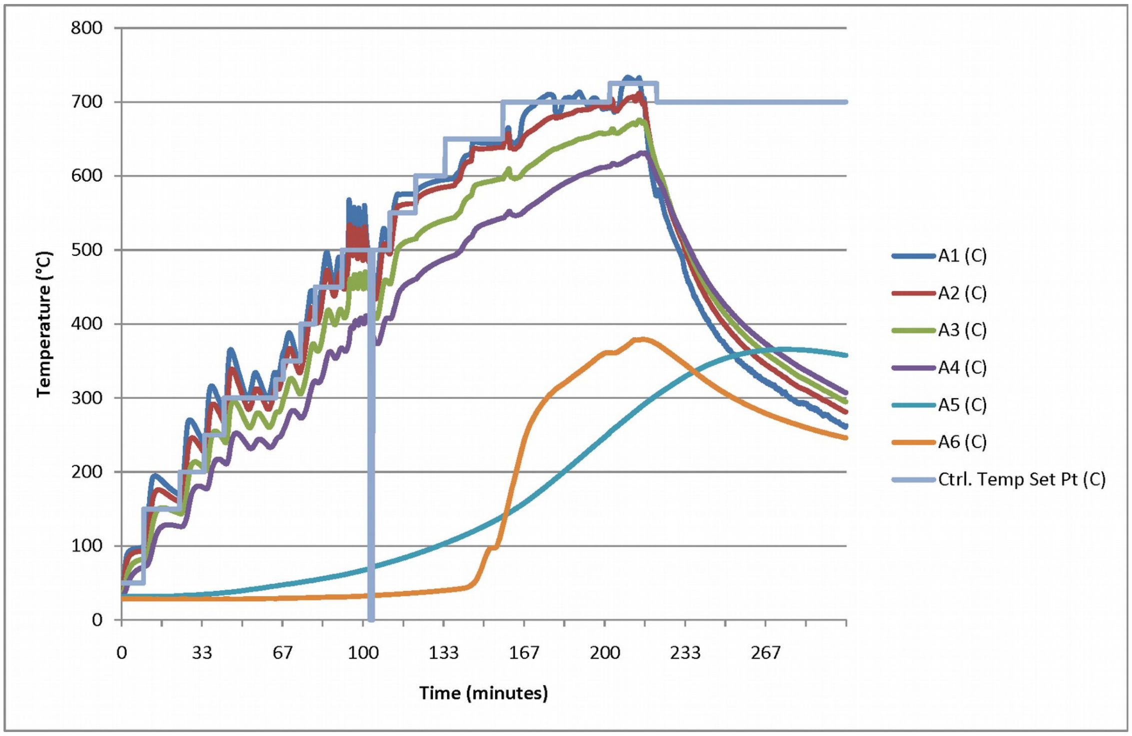

Figure 11, Test #1 Results

On 19 July 2011, the first test was conducted. The plot in Figure 11 below shows the temperatures at positions A1 through A6, as well as the induction heater control temperature set point.

From the plot, the temperature set point was initially set to 50°C, and stepped up over time while maintaining the temperature difference from A1 to A4 to not greater than 100°C. The temperature fluctuations seen at locations 1 through 4 are due to the temperature controller being improperly tuned. At just over 100 minutes, the test was temporarily stopped to correct the problem.

The temperature at the heater head vapor chamber (position 6) lagged at the receiver vapor chamber (position 1) dramatically until the receiver temperature reached approximately 650°C. At that time, the heater head temperature begins to increase rapidly. There is a small plateau at approximately 100°C at location 6, indicative of the sodium phase change. The temperature at location 6 then begins to level off. Next, the control temperature was set to 725°C. At this temperature, the heater head vapor chamber lagged the receiver vapor chamber by approximately 350°C. This is an indication that the heat pipe is not fully functional in transferring heat to the heater head. During this time, the temperature at the vessel mid-plane (position 5) steadily increased, indicating gradual heat-up of the TES salt.

At approximately 220 minutes, a loud buzzing or popping noise was heard coming from the test stand safety enclosure. Power to the induction coil power supply was cut-off immediately, and the test was stopped. The cause of the noise is unknown, and visual observation was not possible due to the all-steel safety enclosure surrounding the TES module and engine housing assembly.

Initially, two explanations were proposed: the first is that the TES module grew due to thermal expansion, and contacted the inductor coil. Although the inductor coil is coated in insulating ceramic, it was thought that perhaps the coil somehow arced to ground through the TES. This scenario was dismissed, since the power supply over-current protection did not trip.

A second theory is that the coolant flowing through the inductor coil leaked out under pressure through a crack or pinhole. Relatively low temperature fluid impinging on the 725°C receiver could result in thermal shock, and account for the popping sound as the coolant flashes to vapor. A subsequent leak check of the coil did not reveal any leak path, however. The coil was pressurized with shop air to about 90 psi, and immersed in water. No bubbles were observed.

The TES module was removed from the test stand and examined. The receiver plate sustained some discoloration and minor surface damage, a photograph of which is shown in Figure 12. The damage to the receiver was judged to be superficial, and ready for further testing.

Test #2 - The test stand was set up as before, with the exception of setting the gap between the receiver and the inductor coil to 6 mm. During Test #1, the gap was initially set at approximately 3 mm. Thermal expansion will cause a structure growth of up to 4 mm, potentially contributing to the incident which caused the damage.

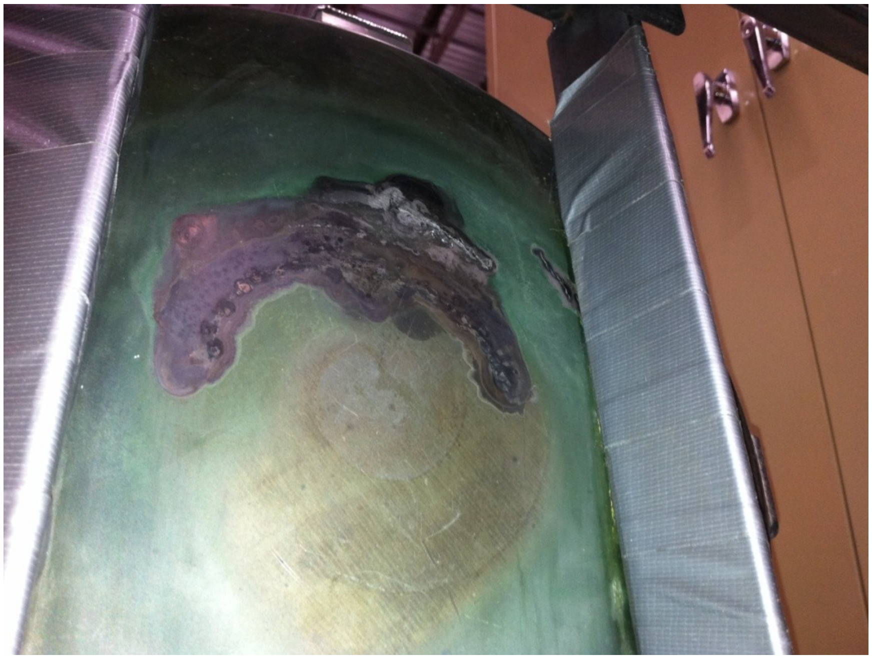

Figure 12, Test #1 Receiver Damage

On 23 August 2011, the second test was conducted. The plot in Figure 13 below shows the temperatures at positions A1 through A6.

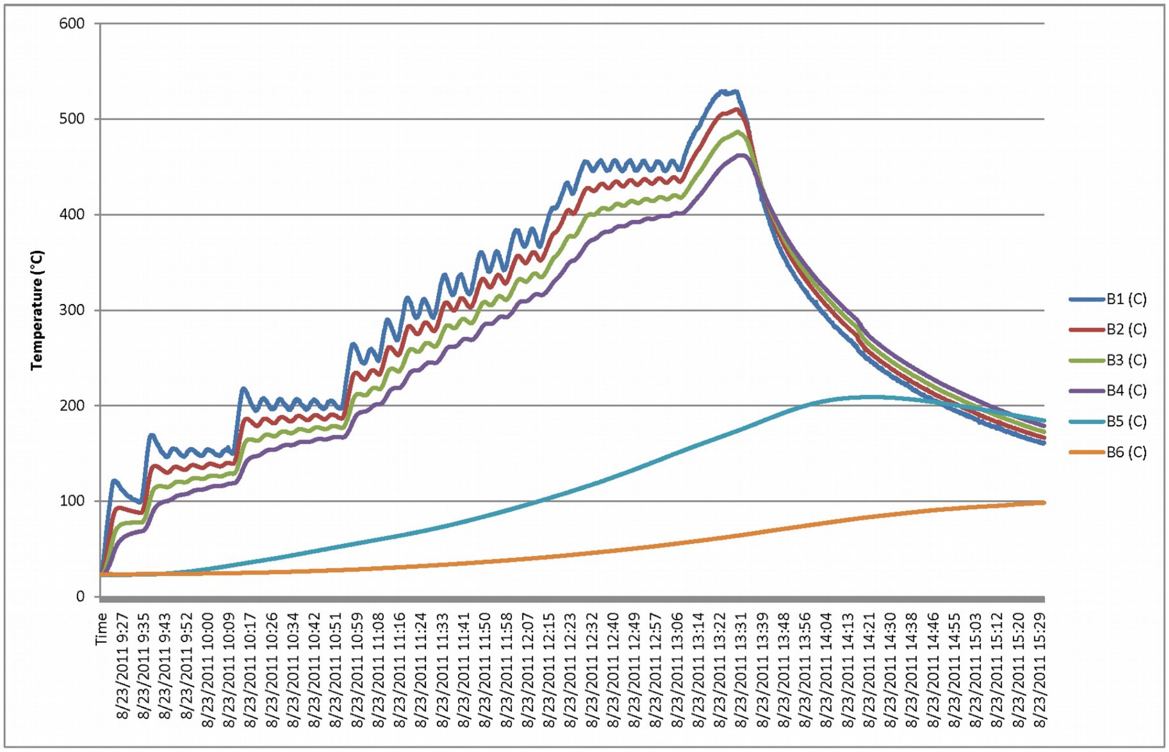

Figure 13, Phase 1 Test #2 Results

As before, the temperature set point (not shown) was gradually increased over time while maintaining a temperature difference between positions 1 and 4 below the 100°C threshold. At approximately 13:30 hours, smoke was observed emerging from the safety enclosure, and the test was immediately stopped.

After a short cool-down period, the safety enclosure was opened. Upon investigation, it was determined that a small quantity of an unknown substance located between the receiver and inductor coil was burning. The substance was dry, fluffy, and resembled popcorn. A photo of the findings is shown in Figure 14.

Over the space of a few hours, the unknown material became foamy. A small sample was collected from the bottom of the safety enclosure for later analysis.

The TES module and engine housing assembly was removed from the test stand. Some metallic-appearing material was collected from the coil and was combined with water outdoors. The sample reacted violently, confirming the suspicion that the receiver had breached and leaked sodium.

Figure 14, Unknown Material, Post-Failure

The photograph of Figure 15 shows the TES receiver plate surface. At the 10-o'clock position, a small lump of solidified sodium can be seen, surrounded by the unknown, foamy material. At the 9-o'clock position, a crack measuring approximately 20 mm in length is seen. Dried green residue resembling the color of propylene glycol – the coolant flowing through the induction coil – surrounds the area of damage.

A team was assembled to determine the root cause of the failure and recommend follow-up action, summarized in the following discussion.

The team constructed a fault tree to guide the investigation, as shown in Figure 16. Four main categories of possible failure were identified:

1. Test Stand – Issues related to the testing set-up or hardware;
2. Receiver Plate – Issues related to the receiver design and/or material;
3. Heat Pipe – Issues related to the heat pipe network design and function;
4. Test Parameters – Issues related to the test plan/protocol.

A number of sub-categories were developed under each main heading. The goal of the team was to investigate each of the potential causes, either rejecting or accepting them based on the evidence uncovered.

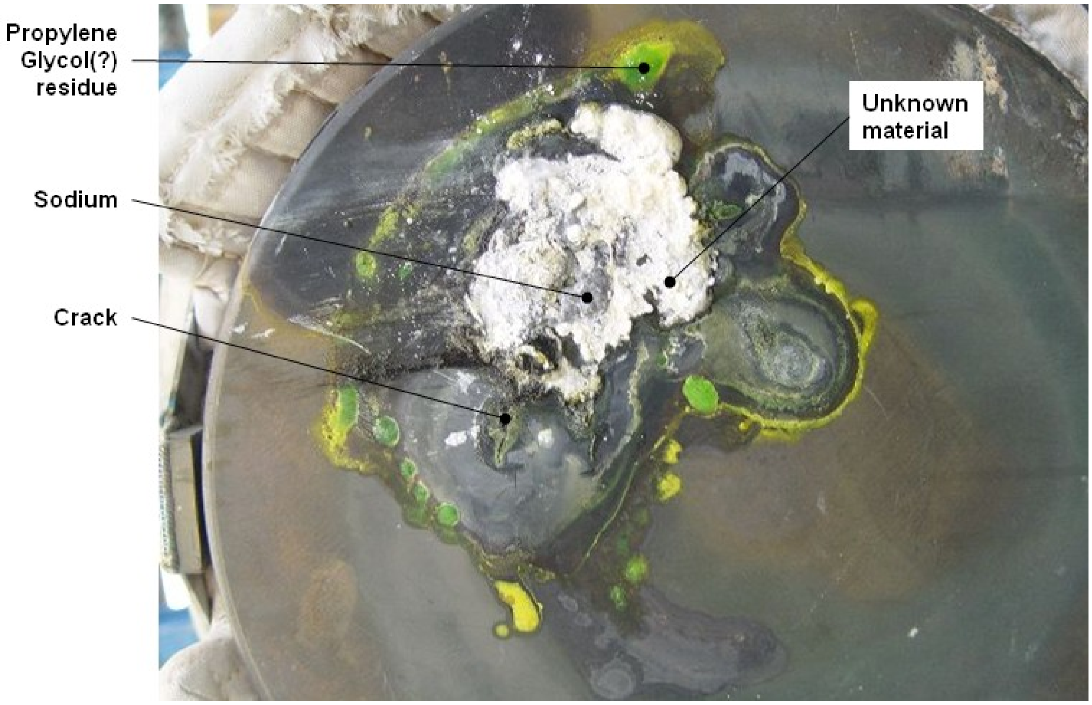

Figure 15, Receiver Face, Post-Failure

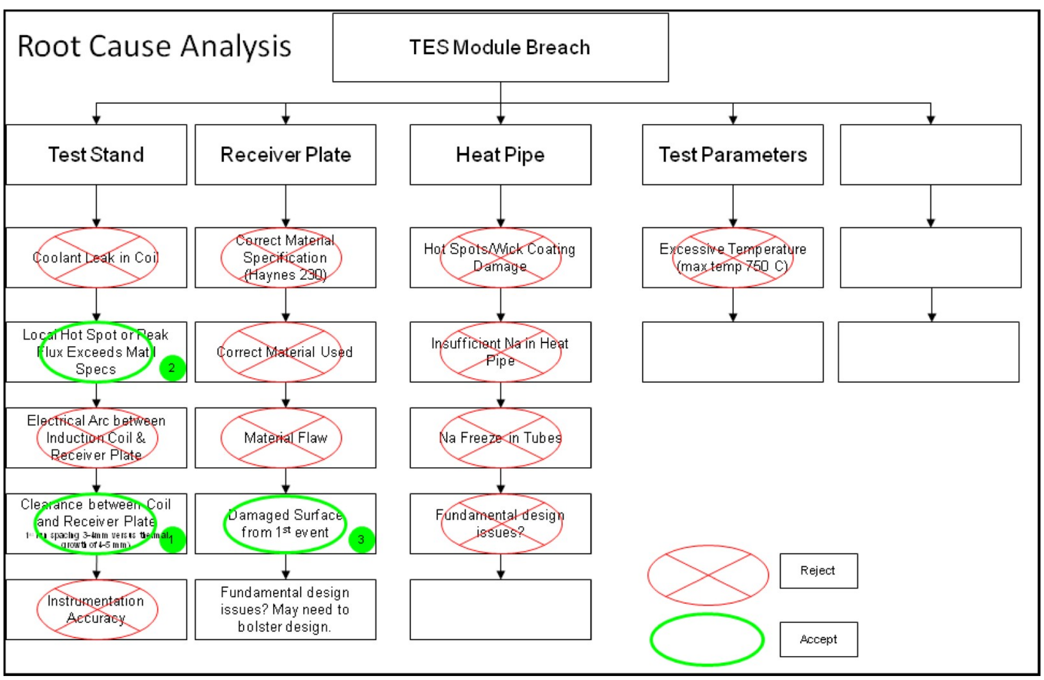

Figure 16, TES Failure Fault Tree

Each of the accepted contributing causes (fault tree sub-categories) is discussed as follows.

Local Hot Spot or Peak Flux Exceeds Material Specs - Damage to the receiver occurred in two discrete locations, leading to the theory that localized high heat fluxes and resulting hot spots led to the crack failures. To test this idea, the receiver plate was removed from the TES module and specimens removed from it for metallographic analysis.

Thermacore was responsible for removing the sodium in the heat pipe network and machining off the receiver plate. The plate was then sent to Infinia for sectioning. The sectioned samples were mounted and analyzed by Thermacore's in-house material scientist. Thermacore's report is excerpted as follows.

Three metallographically mounted and prepared sections of the failed prototype collector plate were received for examination and interpretation. The three mounted samples represented material taken from a) apparently unaffected material, b) material that had bulged outward, but bore no "scars" nor cracks, and c) the region of one of the two cracks in the collector plate.
The specimens were examined by optical and scanning electron metallographic methods.

a. Unaffected Material

The cross section showing the area that was apparently unaffected exhibited the microstructure typical of Haynes 230, rolled and annealed at 2200°F. There were no areas of defects or unusual structure.

b. Bulged Area

This section showed a variety of structures. There were locations that had the same structure as the unaffected material. However, there were areas of localized grain growth, and areas of heavy grain boundary precipitates. These precipitates form when the annealed material is held for a long time at temperatures of 1800-1900°F, or for a much shorter time at about 2200°F. The presence of a very heavy layer of the carbides indicates high temperature exposure for some time. There were areas of coarse grains, with less carbide being present, as one would expect since the carbides dissolve at temperatures that cause grain growth.

c. Near-Crack Area

There were a variety of microstructures. At the outer surface (away from the wick), there were grains that had not grown, but did exhibit a heavy precipitate film. This is evidence that at this surface, temperatures of less than 2200°F were encountered, but that exposure to somewhat lower temperature for enough time to cause carbide precipitation had occurred. There was no evidence of melting or arcing on the outer surface in the region of the crack. Note that some material may have dropped out of the "scar", and I cannot speak for its structure.

Melting had occurred for some depth below the surface on the wick-side of the plate. The grains on the wick side adjacent to the crack had grown, showed heavy carbide precipitates and evidence of melting.

Away from the crack itself, there were areas where grain growth had occurred throughout most of the cross section, evidence of exposure to high temperature, in excess of 2200°F. These observations indicated that high temperature was encountered in a localized region. Bulging occurred either as a result of stresses above yield at those temperatures, or rapid creep below yield stress due to the high temperatures.

The presence of heavy carbide films is detrimental to several material characteristics. First, it results in lower ductility. The second is that the precipitated carbides consume chromium in the region of the grain boundaries. The depleted layer has reduced corrosion resistance compared to the rest of the material. This provides an interconnected corrosion path that can lead to localized failure.

It appears that temperature excursions occurred, producing temperatures that were well above those anticipated in localized regions.

It is clear from the metallurgical analysis that in the area of the crack(s), and in one of the areas where localized yielding occurred, very high temperatures of up to 2200°F (~1200°C) were encountered – well in excess of the design temperature of 750°C.

Clearance between Coil and Receiver Plate - The standard air gap between the induction coil and heater head employed in Infinia engine tests is 3-4mm. This gap gives good inductive coupling for heating, while ensuring that case motion amplitude from the engine's vibration will not allow contact with the coil.

This standard gap was used in the first test run of the TES module. Unfortunately, the thermal expansion of the module was overlooked. Subsequent finite element analysis of the receiver under operating conditions shows that the receiver itself takes on a "dome" shape of several millimeters at its peak. This is problematic since the efficiency of inductive coupling is inversely proportional to the square of the air gap between the coil and target. That is to say, the heat flux increases dramatically as the gap narrows.

This is a well-established characteristic of inductive heating, and was accepted by the team as a contributing factor to the failure.

Damaged Surface from First Event - This investigates the likelihood that the cracked structure resulted from prior damage incurred in the first testing incident.

As the accompanying photo in Figure 17 shows, there is a strong indication that surface damage documented after the first event corresponds to the same location of the breach. Thus, the prior incident likely precipitated the ultimate failure.

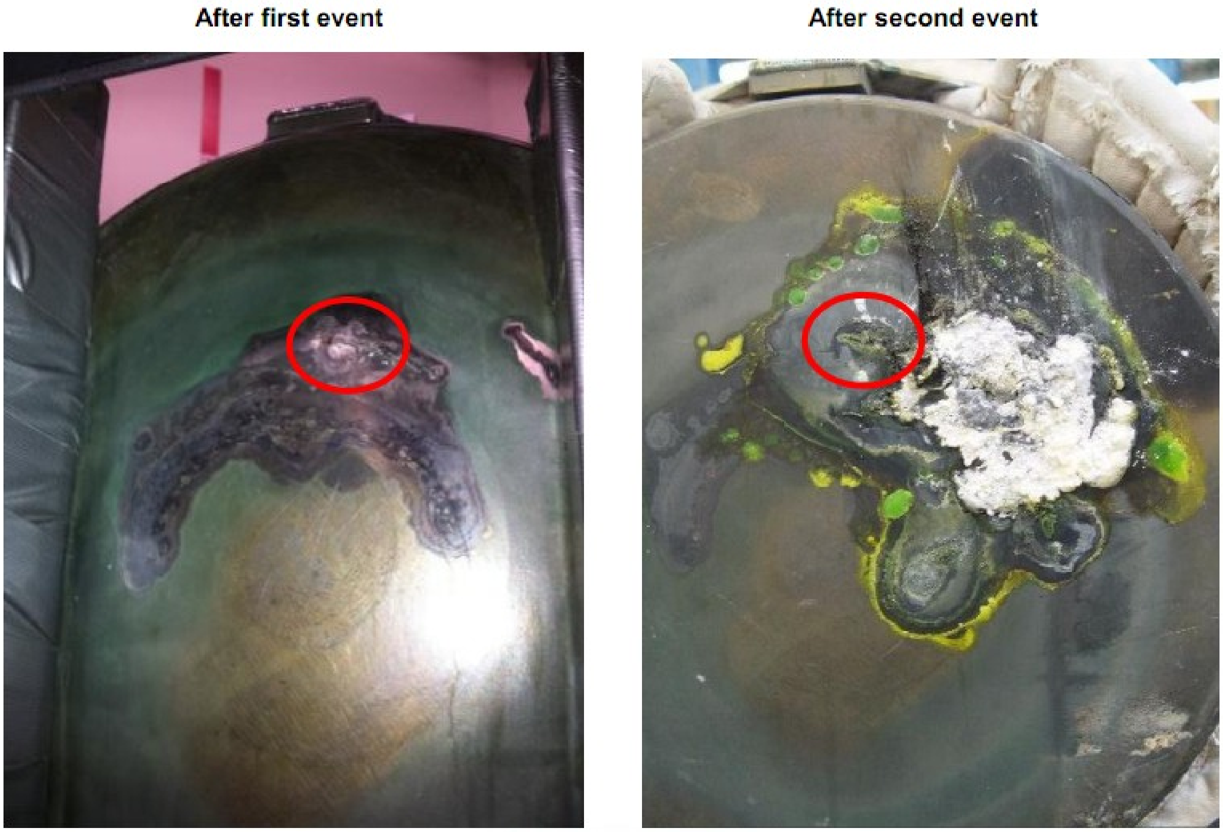

Figure 17, Previous Damage at the Breach Site

Failure Analysis Conclusions - The team came up with fourteen possible root causes, of which three were identified to be probable contributors based on the subsequent investigations. These three were further ranked in order of importance as follows:

1. The gap between the inductor coil and receiver was initially set too small to accommodate the thermal expansion of the TES module during testing. As the air gaps closed, this likely resulted in high heat flux causing…
2. A local hot spot which exceeded the material limits of the receiver and…
3. Damaged the receiver during the first test, which served as the origin of the final breach failure.

Recommendations going forward include:

a. Switch to susceptor-based heating.
b. Place thermocouples directly onto the receiver surface.
c. Verify the suitability of the current receiver design via a suitable FEA model using the best known flux distributions.

These recommendations were implemented in the rebuild and re-testing efforts.

Test #3 - In Task 5, the TES module was repaired by replacing the damaged receiver with a duplicate of the original design, followed by a high-temperature bake-out and sodium fill of the heat pipe region. The module was then shipped to Infinia for testing.

The first task before module testing was to attach K-type thermocouple instrumentation to the exterior, and wrap the TES vessel with high-temperature heat tape. This heat tape was used to pre-heat the TES module to above the melting temperature of sodium (98°C) as needed to avoid heat pipe freeze-out.

Prior to attaching the heaters as discussed above, thermocouples are placed on the TES vessel in order to monitor temperatures. A drawing of the locations of the thermocouples is shown in Figure 18 . These thermocouple locations are referred to extensively in the testing results and are discussed in the following. Thermocouple (TC) 1 and 2 are on the face of the TES receiver. Their locations were chosen to correspond with the radial locations of the hottest two susceptor rings, as determined by the induction coil manufacturer's computer aided simulations. Location TC 3 is axially centered on the receiver heat pipe vapor chamber (HPVC) exterior, while TC 4 is located 1 cm from TC 3, in the area of the salt canister closest to the receiver HPVC. Location TC 5 is axially centered between the receiver and engine heater head HPVCs, while location TC 6 is centered on the heater head HPVC itself. All of the axial locations from TC 3 through 6 are replicated in 4 radial locations, labeled A, B, C and D. Radial location A is 45° clock-wise from the 12 o'clock position. Radial locations B, C and D are spaced at 90° respectively. There are therefore 16 TES vessel temperatures being recorded, aside from the receiver TCs, referred to as 3A, 4A, 5A and so on through 6D.

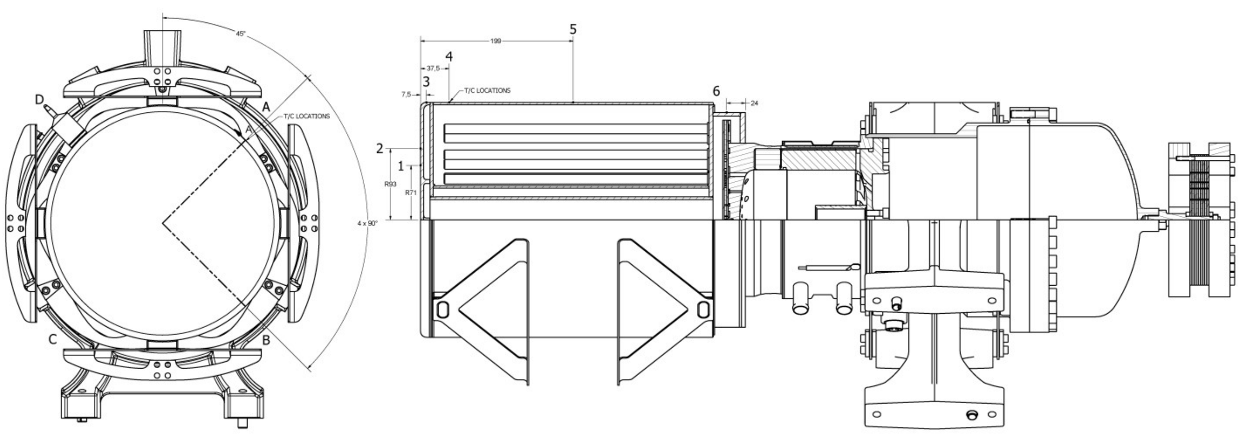

Figure 18, Thermocouple Locations

Test Procedures - The TES module was connected to a data acquisition system (DAQ), which was equipped with virtual instrument (VI) software. The VI is used to monitor and record test data such as temperature, engine power and susceptor parameters. The VI interface is also used to control susceptor power input and to control engine stroke.

The test plan developed involves two phases. In Phase I, the engine is rendered inoperative by evacuating the helium working fluid. Then, the heaters are used to charge the TES salt mass. In Phase II, the engine is charged with helium and the TES is charged as before, while the engine is allowed to run. The two testing phases are summarized below.

Phase I: Initial start-up testing:

1. Pre-heat the vessel to 300°C using the tape heaters. Allow to heat-soak overnight. Turn off heat tape, start susceptor heating at 400°C input. Monitor temperatures T_3 and T_4. Differential shall not exceed 100°C. If this level is reached, reduce temperature set point. When differential reaches 60°C or less, increase setting 100°C and monitor. Repeat until receiver face temperature of 800-850°C is achieved at T_1 and T_2; allow entire vessel to reach steady state, such that temperatures at T_5 are 700°C or greater . Stop the test and record results. Engine shall remain inactive (no helium) during this test.

Phase II: Test full system:

1. Charge engine with helium. Charge salt volume to 750°C. Keep engine at lowest possible part load.
2. Map engine performance down to 450°C: Range from maximum output to 3.0kW$_e$, measure charge/discharge time, efficiencies.
3. Charge salt volume as before while running engine at 2.0kW$_e$.

Results - Phase I testing occurred 6 June 2012. The resulting temperature plot is shown in Figure 19 below. Radial TC locations at position “A” were chosen as representative of the test results. Also shown in the plot is the susceptor duty cycle. The duty cycle cannot be used to directly determine power input levels. However, through Infinia’s solar engine testing efforts, estimated power levels are available. As detailed in the test plan, the tape heaters were set for 300°C the day before, and the vessel was allowed to heat-soak overnight.

The susceptor was turned on at approximately 9:00 am. Heat was applied gradually such that a temperature differential of no more than 100°C between locations TC 3 and 4 occurred, to avoid excessive thermal stresses. At around 10:30 am, it can be seen that the receiver temperature reaches approximately 550°C, at which point the heat pipe starts to transfer heat to the heater head HPVC. This is reflected in the rapid temperature rise of TC 6. However, the response at TC 6 then decreases, and finally a more linear trend is seen for the remainder of the test. This is not the desired result. Since the receiver and heater head HPVCs are directly coupled via a large, central heat pipe, it was anticipated that the temperatures at TC 3 and 6 would be nearly isothermal once the heat pipe reached its operating temperature of 550-600°at the evaporator. Unfortunately, a temperature difference of 350-400°C from TC 3 to 6 is indicative that the heat pipe is not functioning properly. The test was continued until just after 7:00 pm; roughly 10 hours. At this time, the salt temperature as measured at TC 5 was only 550°C and climbing slowly. Receiver temperature at TC 1 was pushed to as high as 900°C, corresponding to a heater duty cycle of around 23%. This is an estimated power input of only around 3500 W; nowhere near the desired input level of 11 kW. As the goal was to melt the salt mass by bringing the temperature up to at least 750°C, the test was terminated since it became clear that the device was not working to expectations.

Infinia consulted with TES module manufacturer and high temperature heat pipe experts at Thermacore, Inc. about the test result. Thermacore pointed out that the design intent of the heat pipe system is to split the incoming energy, with about 8 kW transferred to the engine, and 3 kW to the salt, out of a total 11 kW delivered to the receiver. The heat pipes embedded in the salt were thus sized accordingly. Since the system was not designed to transfer full input power to the salt only, Thermacore's recommendation was to proceed to Phase II testing with the Stirling engine enabled. In addition, Thermacore recommended introducing a non-condensable gas (NCG) charge to assist in biasing the energy split to the engine, and allowing the heat pipe network to gradually heat up the salt over time.

Infinia agreed to move on to Phase II testing. Prior to conducting that testing however, the TES heat pipe volume needed to be charged with the proper amount of argon NCG. This was anticipated, and the heat pipe fill tube was outfitted with a bellows valve, instead of being pinched and seal-welded. Thermacore originally designed the TES heat pipe space to contain 2.2×10^{-4} moles of argon. NCG will collect in the cold, quiescent portions of a heat pipe, blocking the heat pipe's sodium working fluid from condensing there and thus blunting heat transfer.

The NCG was deliberately introduced to block heat loss through the receiver during TES discharge. In the absence of sunlight, the receiver becomes cold, and is a path for unwanted heat transfer. During analysis of the TES heat pipe network, a balance was struck between blocking the receiver at discharge, and accepting some level of impaired function during charging. The NCG is compressible, and thus occupies less volume as the temperature and pressure of the sodium vapor increases during charging. By calculation, the NCG charge would fill the central heat pipe, heater head vapor chamber, and secondary heat pipes until about 550°C, at which point only the secondary heat pipes are blocked. Theoretically, the heater head vapor chamber is free of NCG. Further heating to 680°C results in the NCG being compressed into the secondary heat pipe tips. At this condition, the last 10% of the secondary heat pipe's lengths are rendered ineffective.

For the first NCG fill, it was decided to reduce the charge somewhat to 1.5×10^{-4} mol. This was done based on from testing conducted in 2011 that suggested NCG may have interfered with heat transfer to the heater head HPVC. After successfully clearing the sodium from the fill valve, the heat pipe space was evacuated, and the argon charge was introduced. Then, the engine was charged with helium, and the pre-heaters turned on to 200°C overnight.

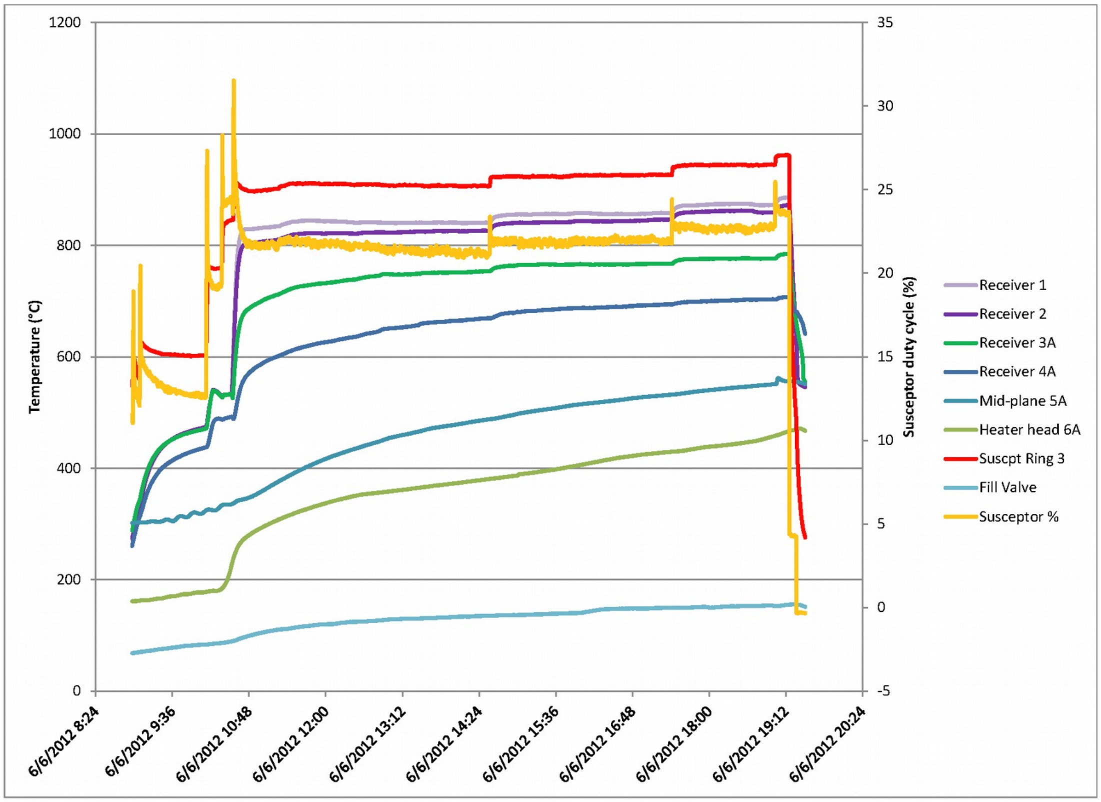

Figure 19, Phase I Salt Melt Testing Results

The first Phase II test was conducted 29 June 2012, results shown in the plot of Figure 20. Again, it can be seen that when the receiver temperature reaches about 550°C, the heat pipe begins to transfer heat energy through the central heat pipe to the engine heater head. Indeed, the red trace, which indicates engine output power, shows that the engine begins generating electricity at this time. However, as before, the temperature differential between the receiver and heater head HPVCs is still around 400°C, which indicates that the heat pipe is not operating isothermally. For much of the duration of the test, the engine output spikes, and then depletes available energy until it cannot continue operating. This cycle continues until around 22000 seconds, at which time there is sufficient thermal energy contained in the TES module to maintain engine output at around 20W continuously. The receiver temperature at this point is about 850°C, with an estimated heat input rate of 3.2 kW. After 8 hours' run time, the TES salt temperature as measured at TC 5 is only 450°C, and the test was terminated.

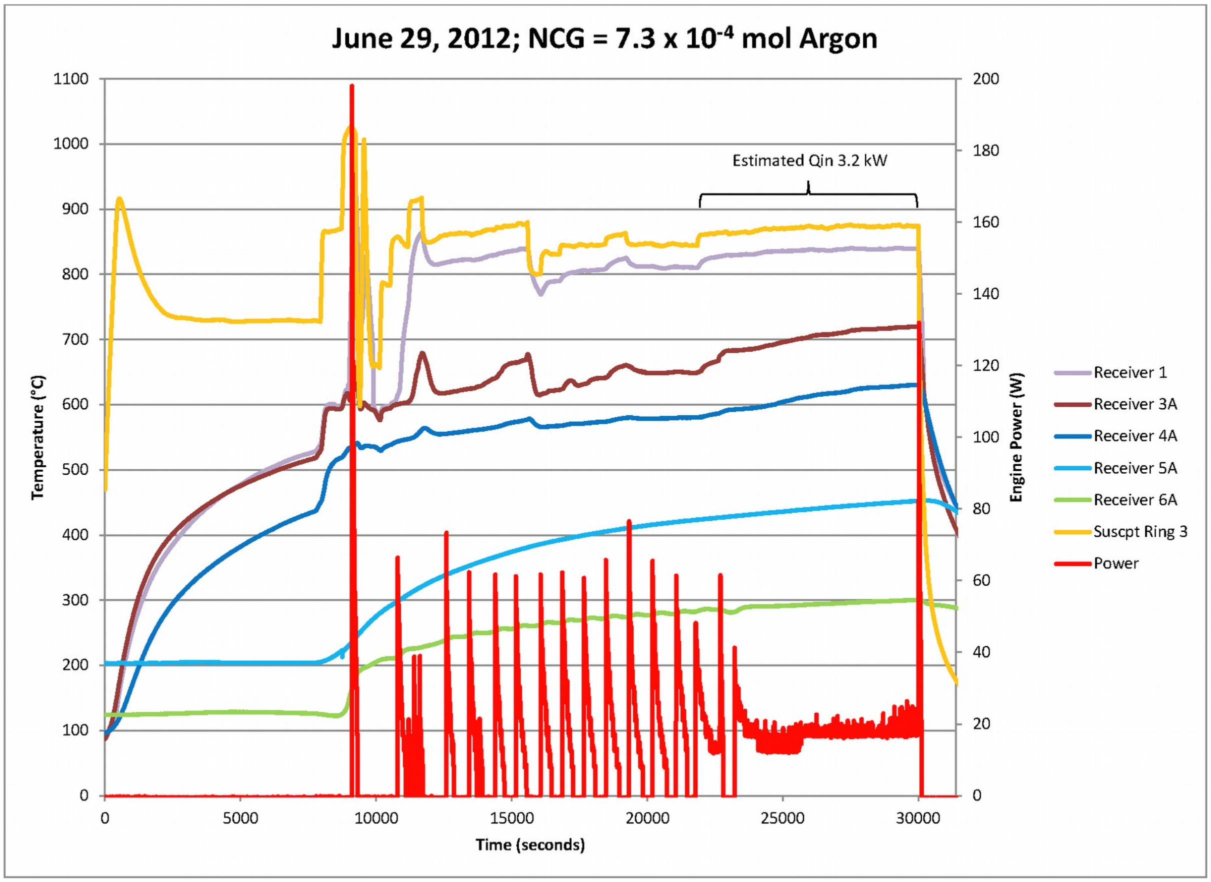

Figure 20, Phase II Full Test Results; 29 June 2012

After reviewing the data from this test, it was decided to try the original argon charge amount of 2.2 x 10^{-4} mol, to see if the performance would improve. The clearing/charging procedure was repeated with a revised charge pressure, and the test repeated on 5 July 2012. The results of this test are shown in Figure 21. It should first be noted that the data recording was not initiated until well after the susceptor heating began. This can be seen in the apparent starting temperature at the receiver of about 400°C rather than 100°C as with the previous test. Also, during this test, the commanded engine stroke voltage was higher than before, which resulted in higher peak engine output spikes. In any case, the results are very similar as before; a large temperature differential between the receiver and heater head, and a limited heat input capacity before the receiver temperature reaches its maximum allowable temperature.

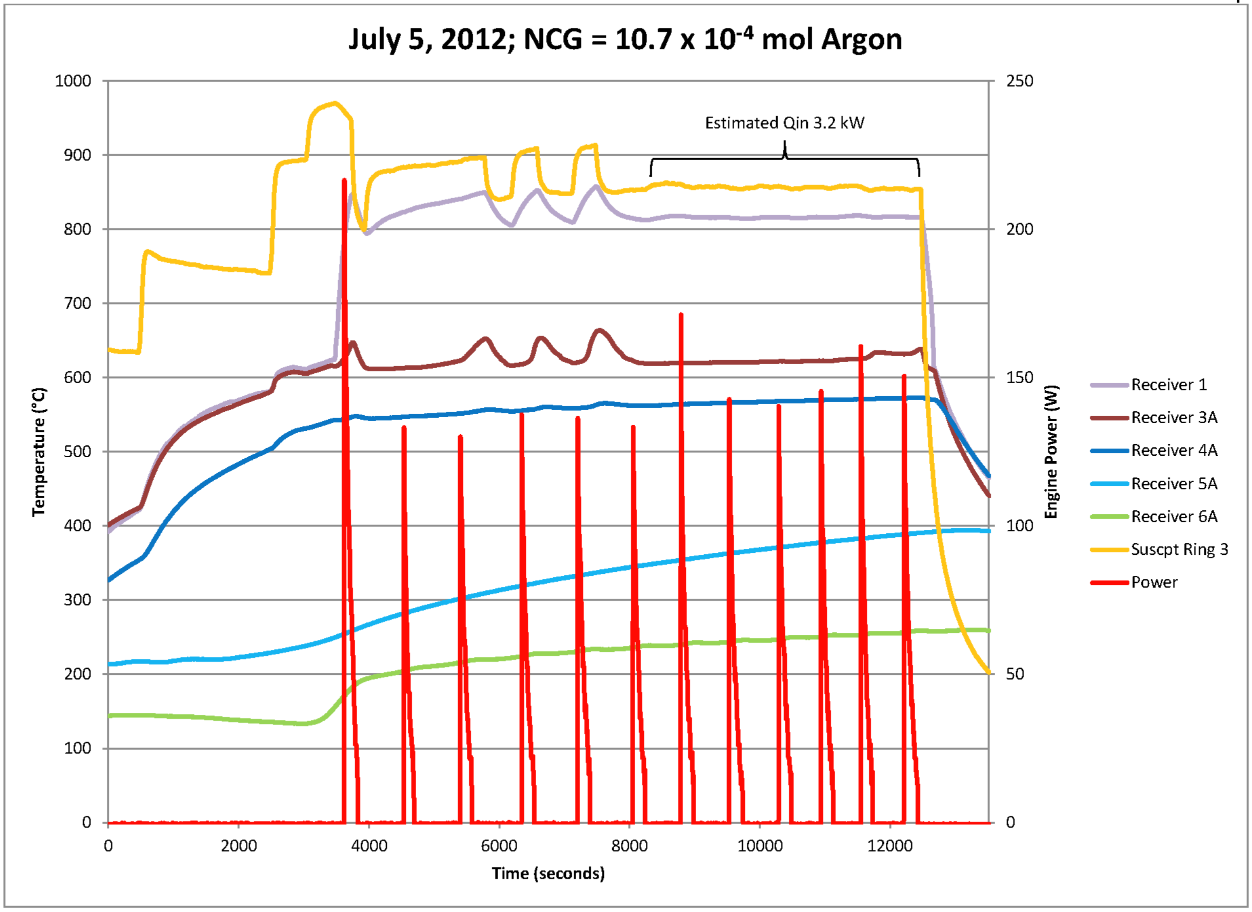

Figure 21, Phase II Full Test Results, 5 July 2012

Thermacore was again contacted to review the results. During the consultation, the argon fill procedure was reviewed. Thermacore pointed out that the pressure calculated in the previous discussion is absolute pressure, and inquired as to whether the charge pressure was determined by absolute or gauge pressure. The pressure used to charge the TES heat pipe network was in fact gauge pressure, which means that the ambient pressure (approximately 12.7 psi in Ogden, UT) was not accounted for. Thus, the charge amounts were significantly higher than previously supposed. These charge amounts are correctly labeled in molar terms in the plots of Figure 20 and Figure 21. Accordingly, and third purge and fill of the TES heat pipe space was conducted, with the appropriate pressure argon charge corresponding to 2.2 x 10^{-4} moles. The third attempt at this test was conducted 10 July 2012, the results of which are given in Figure 22.

As can be seen, although the argon charge is reduced by a factor of nearly 5, the results are remarkably similar to the previous tests. The heat pipe does not operate isothermally as expected, and power input is limited.

At this point, it was decided to try a different approach to the test. As it appears that charging the TES via heating of the receiver does not function properly regardless of NCG charge, the focus shifted to testing the discharge capabilities of the TES module. The tape heaters would be used at maximum power input in conjunction with the susceptor to try to melt the salt, at which time the engine could be run from the salt's thermal energy only. This test would validate at least part of the functionality of the TES module; that of the ability to transfer the heat energy contained in the salt to the engine for the required time period and electrical energy output.

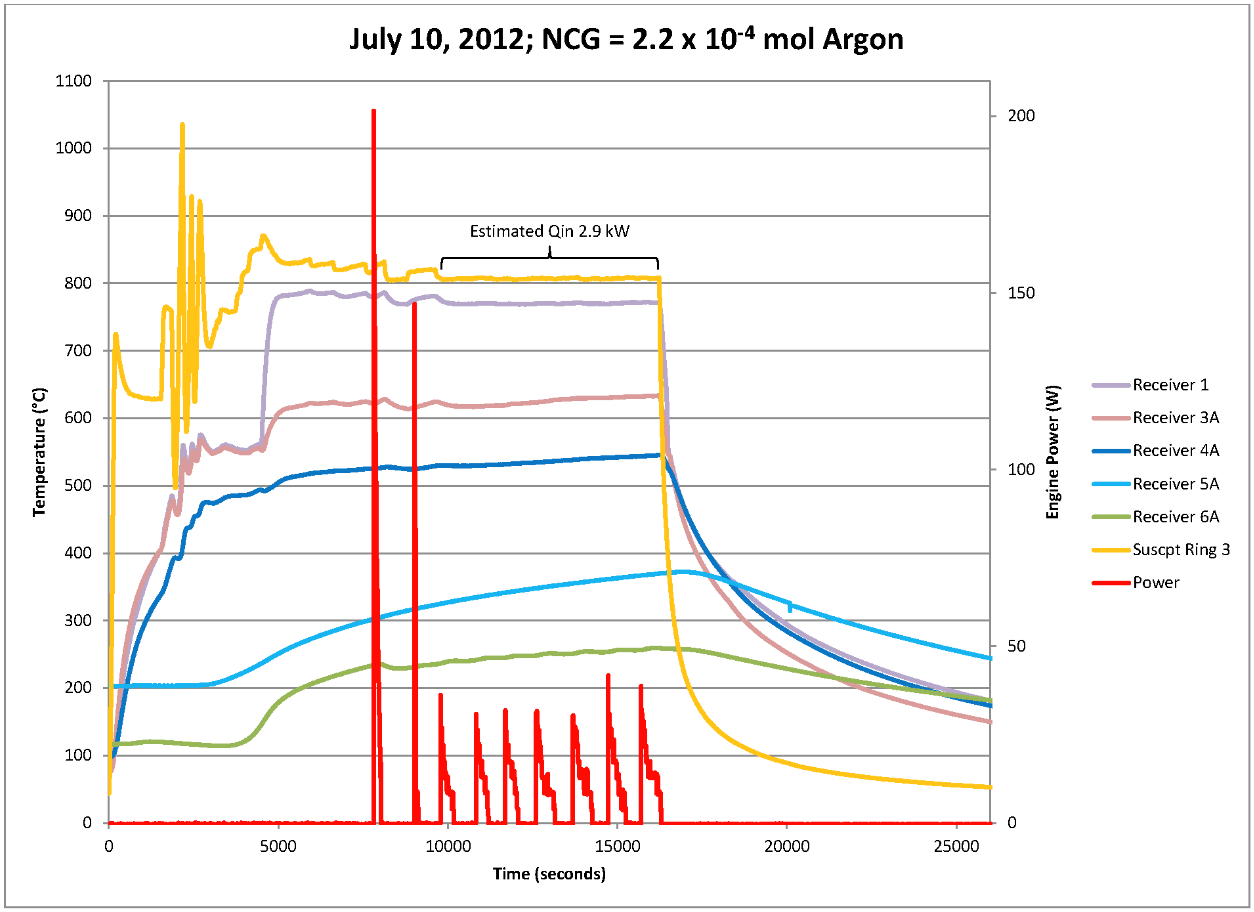

Figure 22, Phase II Full Test Results, 10 July 2012

Before conducting this test, the heaters around the TES vessel were set for 300°C, and the vessel allowed to heat soak overnight. The results of this test are shown in Figure 23.

Yet again, there is an abrupt rise in temperature at the heater head HPVC when the receiver temperature reaches 550-600°C, indicating partial functionality of the heat pipe connecting the receiver to the heater head. At around 5.5 hours, the system is approaching a state of thermal equilibrium, whereby the engine is producing a nearly constant 300 W, while the salt temperature at TC 5 stays at around 500°C, climbing very slowly. There is still a significant temperature differential of about 300°C between the receiver and heater head, and the receiver temperature is at around 850°C at an estimated susceptor input of 3.5 kW. The tape heaters are running at full power; two heaters at 1250 W apiece, for a total input energy rate of about 6 kW. Again it is clear from the data that melting the salt will not be possible – at least within a reasonable time frame – and the test is stopped. However, before terminating the heat input, the engine stroke is increased, to see what the effects are.

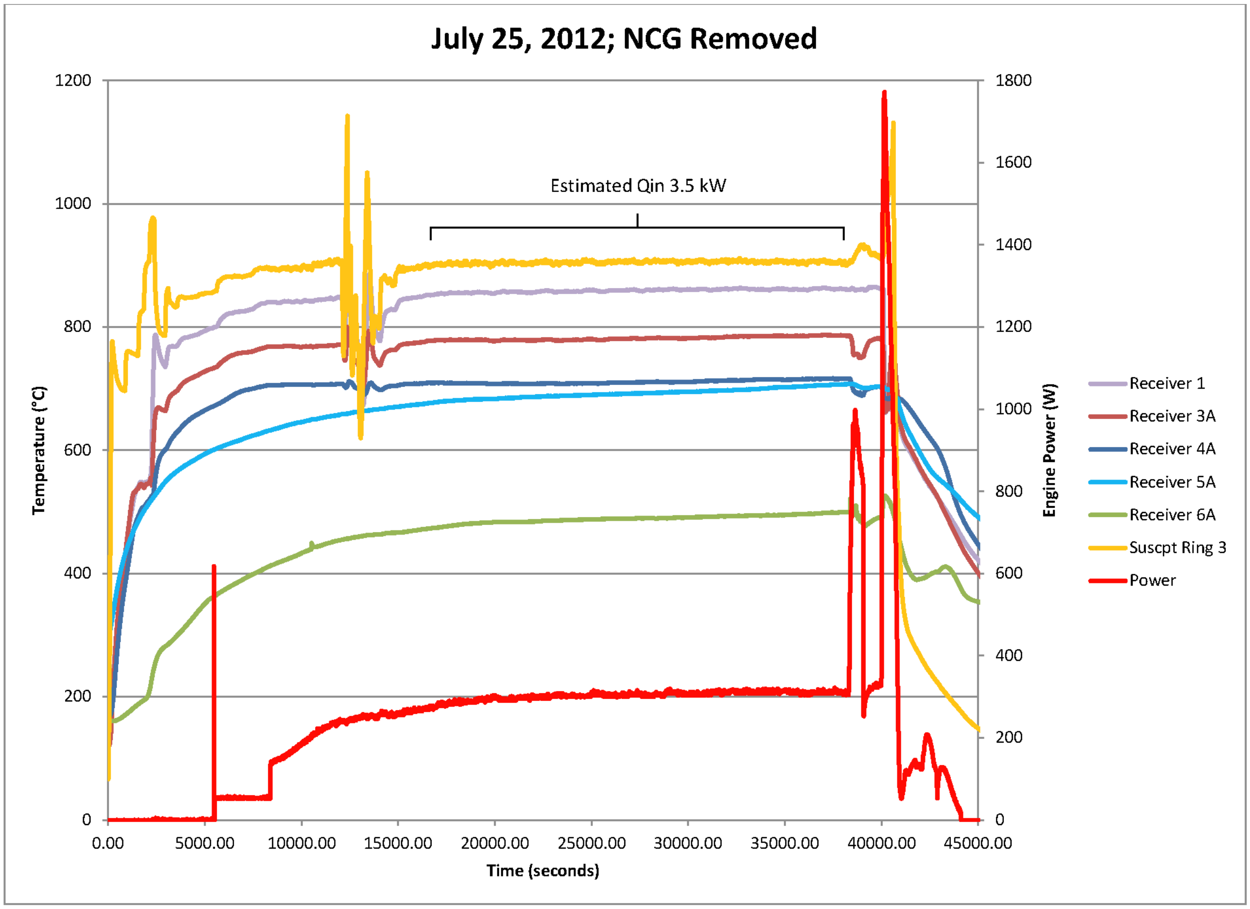

Figure 23, Modified Phase II Test Results, 25 July 2012

The result of increasing the engine stroke, which has the effect of extracting more energy from the sodium space, is that the heater head heat pipe vapor chamber temperature increased slightly. This appears counterintuitive, as pulling energy out of the system should result in lower temperatures. A possible explanation for this is that by pulling more energy out of the system to the engine, the energy split between the salt and engine is more heavily biased to the engine. The heater head will be cooler than the salt, and so more hot sodium vapor will flow to that area, temporarily increasing the local temperature. Interestingly, the receiver temperature did not decrease as would be expected. Theoretically, cooled sodium from the heater head area should flow to the evaporator (receiver), causing the temperature to drop, so long as the susceptor power level is maintained. This did not occur; a further indication that the heat pipe functionality is somehow impaired. To conclude the test, full engine stroke was commanded, resulting in an output spike of almost 1.8 kW. Then, all heaters were shut down. The engine power decreased rapidly from its peak, but then recovered slightly for a short time. By looking at the heater head vapor chamber temperature at location TC 6, it can be seen that the engine power level corresponds to a short plateau in temperature. This activity may be indicative of a small amount of latent heat extraction from the salt, some of which could have become molten during the heating phase.

After this last test was run, it was decided to repeat the test using more external heat applied to the vessel exterior. Although Infinia procured three tape heaters, only two were used for pre-heating. The TES module was removed from the test stand, the insulation removed, and a third heater wrapped around the vessel for a total of 3750 W of maximum heat tape capacity. Also at this time, the receiver was inspected to evaluate its condition after repeated use at temperatures up to 900°C. The receiver appeared to be in good condition, with no evidence of significant deformation or other damage.

The test was conducted 31 July 2012, with the results given in the series of plots shown in Figure 24 through Figure 27. In Figure 24 below, the temperature and engine power plots are shown from the time at which the susceptor was started, through 10 hours' time. The tape heaters were left on overnight at 300°C, and then the heater set point was raised to 750°C in the morning. Throughout much of the testing, the susceptor supplied an estimated 2.8 kW to the receiver, with the receiver temperature staying within a narrow range around 850°C. During most of this test, engine stroke voltage was commanded to the lowest permissible value to minimize energy extraction by the Stirling cycle. However, on three occasions, the engine stroke was varied to examine the effects on the system. Various time intervals of interest during this test are covered in the Figures and discussion that follow.

The time interval from 0-90 minutes (Figure 25) reveals some interesting details about the test. As has been noted in all of the previous tests, it can be seen that when the receiver reaches a temperature of about 550-600°C, the heat pipe begins to function, and heat is transferred to the heater head HPVC as indicated by its rising temperature. Also notable is the temperature divergence of the thermocouple located on the receiver and the thermocouple(s) located at position TC 3. This also occurs at the point in time where the heat pipe appears to start transferring energy to the engine. In a properly functioning heat pipe, the expectation is that these temperatures would be very close. When the evaporator temperature is high enough, the sodium vapor pressure increase causes the sodium vapor to travel to lower temperature, lower pressure areas, where it condenses. The divergence of temperature suggests that sodium condensate cannot return to the flat face of the evaporator fast enough, and the temperature increases. Prior to the heat pipe becoming "active", it can be seen that the engine heater head temperature increased enough that the engine self-started. Initially, the engine stroke was kept to minimum levels. When the heater head HPVC temperature began to rise as a result of the heat pipe starting to function, the engine stroke was increased. Power output spiked, but quickly came back down. Engine stroke was again increased with the same result two more times before being brought back to the minimum.

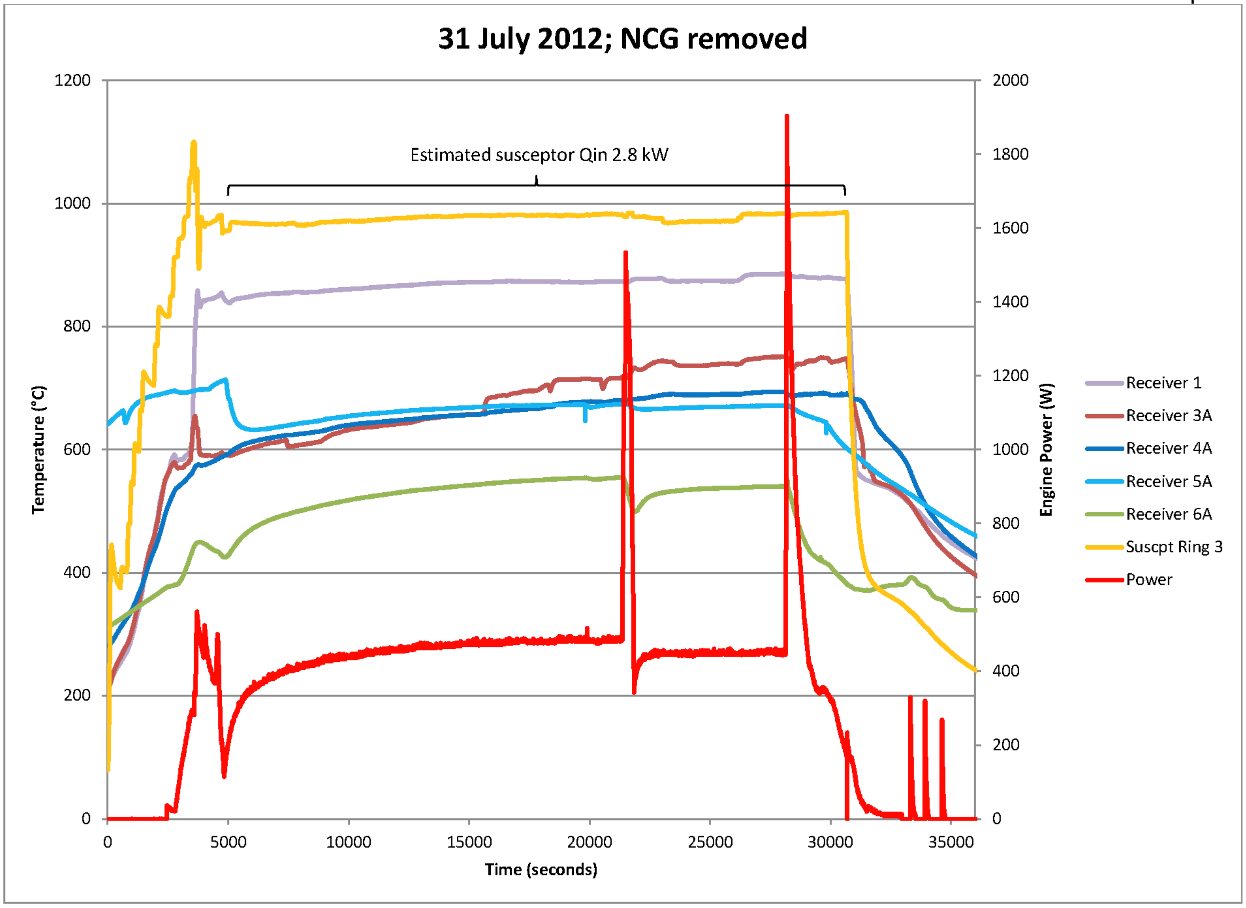

Figure 24, Modified Phase II Test Results, 31 July 2012

This temporarily suppressed the heater head HPVC temperature as expected, but also resulted in a short-term spike in the receiver temperature at locations TC 1 and 3. This again suggests a deficit of return condensate; as the engine consumes more energy, a higher mass flow of sodium vapor is required to support the heat transfer. As this sodium condenses on the engine heater head, the liquid must find its way down the central heat pipe to the evaporator. This is a gravity-aided situation, but it may be possible that some fraction of the liquid makes its way down the many secondary heat pipes - which are embedded in the salt – instead. The final observation during this time period is that as the engine begins to generate more power, the temperature of the thermocouples at locations TC 5 starts to fall. This is likely because the outer row of secondary heat pipes are within 25mm of the TES vessel exterior, and are able to extract heat energy form the tape heaters through the salt layer.

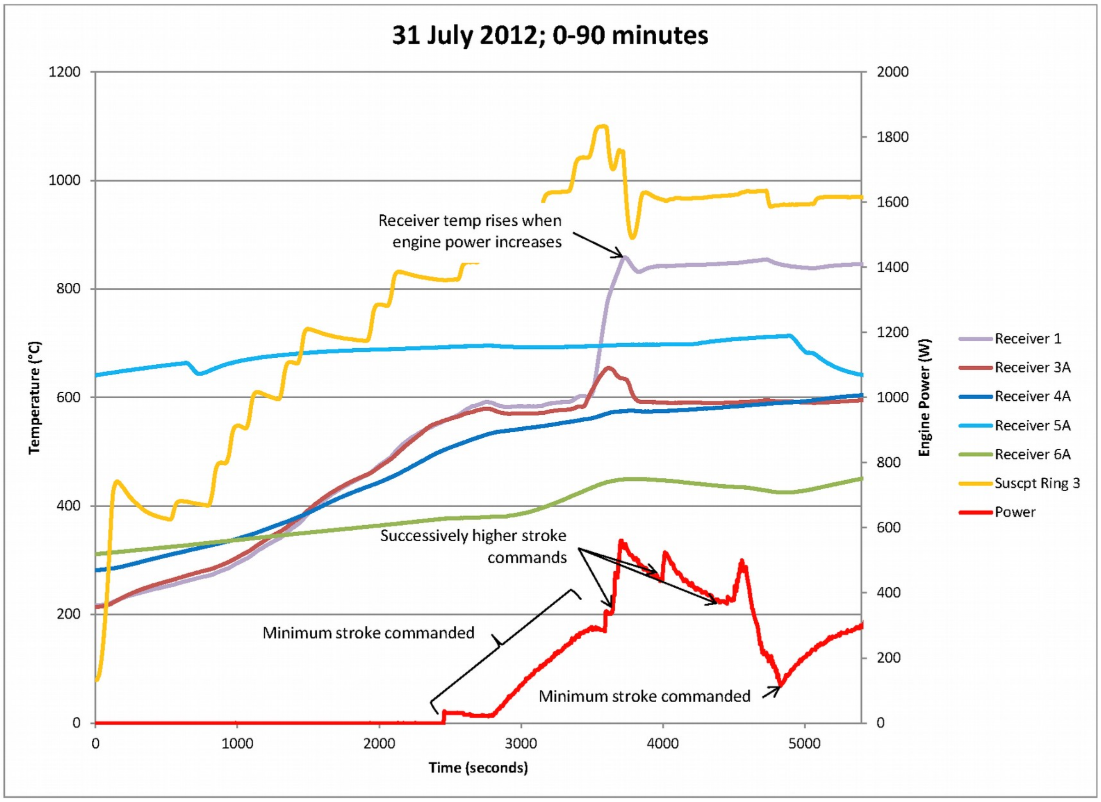

Figure 25, Test Results, 31 July 2012; 0-90 Minutes

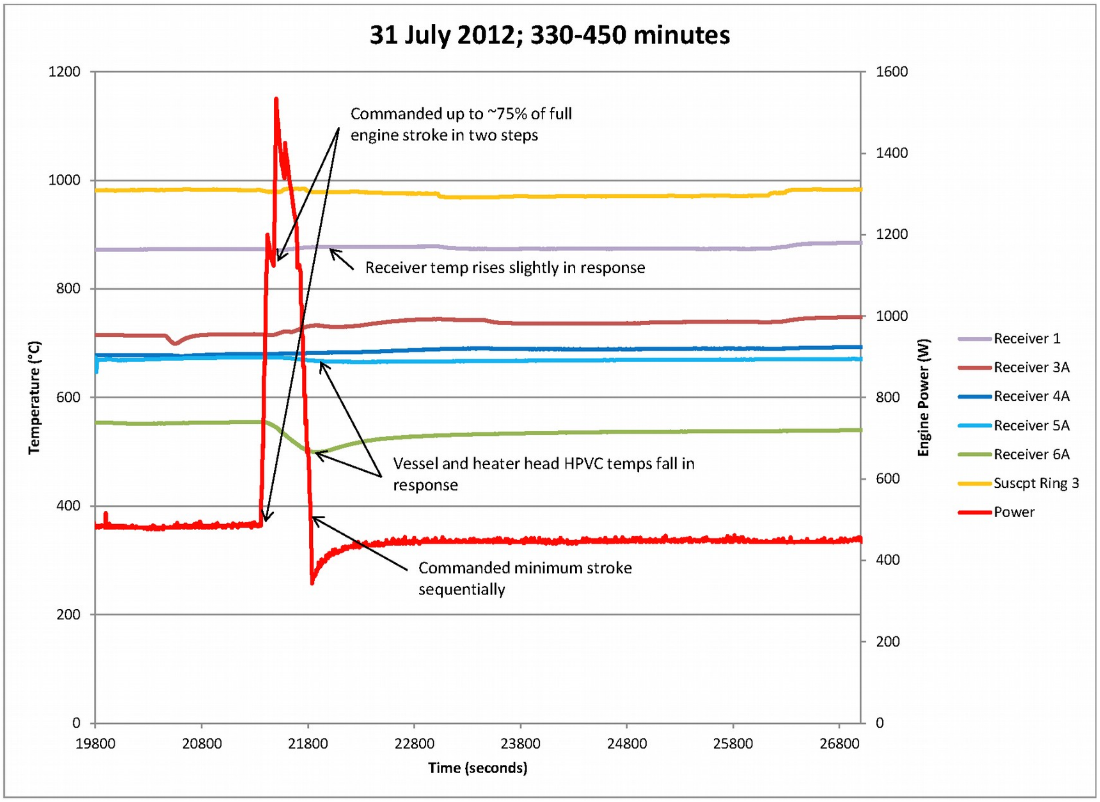

Figure 26, Test Results, 31 July 2012; 330-450 Minutes

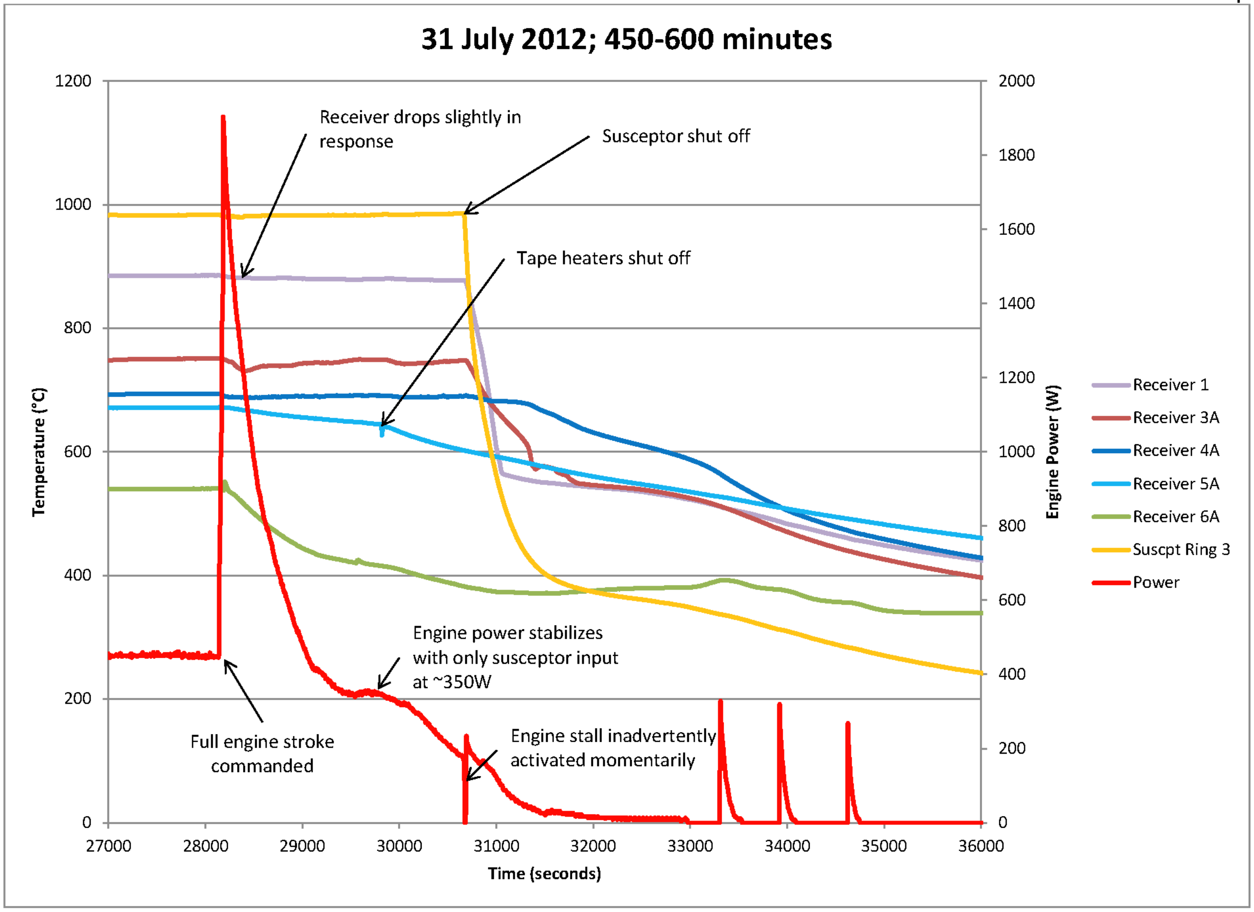

Figure 27, Test Results, 31 July 2012; 450-600 Minutes

The next 4 hours saw temperatures gradually increase until the system neared thermal equilibrium. Figure 26 shows the result of suddenly increasing engine stroke; first to about 60%, and then 75% of maximum. Engine output power reached approximately 1550 W, while the heater head HPVC and vessel saw a decrease in temperature. Although more subtle, the engine power output increase also resulted in slight increases in the thermocouple on or near the receiver at locations TC 1, 3 and 4; further supporting the notion that condensate return may be impaired. The commanded engine stroke was then set back to its minimum value.

After allowing the system to recover, full engine stroke was commanded. This was left in place for the remainder of the test. Interestingly, this time the receiver temperature dropped slightly. After spiking to about 1900 W, engine output power stabilized to about 350 W. Shortly after, the tape heaters were shut off. This caused the engine output to immediately drop, as well as the temperature at location TC 5. This drop in power and temperature indicate that the engine was drawing substantial energy from the tape heaters, rather than from the receiver via the heat pipes. After engine output had dropped to 200 W, the susceptor was shut down. It should be noted that the test stand features two emergency stop buttons; one for stopping the heater only, and one for stopping the heater and activating the engine stall circuit. The latter button was pressed by mistake, when the intention was to simply turn off the heater. The engine was quickly restarted, which is the cause for the momentary drop in engine power output and recovery. The engine continued to run for a short time, with power output falling continuously until the engine stopped at around 33,000 seconds. On three separate occasions thereafter, the engine spontaneously started and quickly ran down, due to a build-up of thermal energy at the heater head. Another notable plot is that of the heater head HPVC. The temperature remained mostly stable at 350-375°C for approximately 40 minutes after the susceptor was turned off. This suggests that some portion of the TES salt became molten during the test, causing the temperature to plateau during salt solidification.

These test results fell well short of expectations. The heat pipe network does not transfer sufficient energy to the engine/salt to heat and melt the salt before thermal equilibrium occurs; in part because the engine eventually begins to extract energy from the system. Attempts to augment the susceptor with tape heaters also were not entirely successful, although there is evidence that some small fraction of salt could be melted using this method. It was decided to attempt to melt the salt mass by using the tape heaters and susceptor together when the Stirling engine is evacuated of helium working fluid (disabled). This eliminates the extraction of thermal energy by the engine while charging is underway. Then, when the salt becomes molten, the engine will be slowly charged with helium, and allowed to start.

The next test was conducted August 7, 2012. Prior to the test, the engine was evacuated, and the three tape heaters energized to pre-heat the TES module to 200°C overnight. The results are shown in the plots of Figure 28 and Figure 29.

At the beginning of the test, the tape heaters were set to full power by increasing the temperature set points to 750°C. The susceptor was ramped up to a maximum of approximately 3500 W. At approximately 2 hours, the salt began to melt as evidenced by a temperature plateau of 680°C. The melt phase duration was about 1.5 hours before the salt eventually reached a superheated temperature of about 750°C. The tape heaters and susceptor were then shut off.

At this point, the engine was pressurized with helium which resulted in the engine self-starting. The output power spiked to 2000 W, but immediately begins to decline. A higher stroke voltage was commanded, which resulted in a temporary bump in output, which can be seen in the detail plot of Figure 29. It can be seen that the heater head vapor chamber temperature drops immediately in response to the extraction of energy from the salt by the engine. This would indicate that the salt rapidly solidifies around the heat pipes, creating an insulating layer that impedes heat transfer. The heater head temperature stabilized somewhat during the salt latent heat extraction at an engine output of around 400 W. Eventually, the salt solidifies completely, during which engine power steadily declines to zero. There were a couple of small power spikes resulting from thermal energy building up at the heater head before being dissipated. The total electrical energy generated during this run was approximately 900 W-h; about 30% of the 3 kW-h goal.

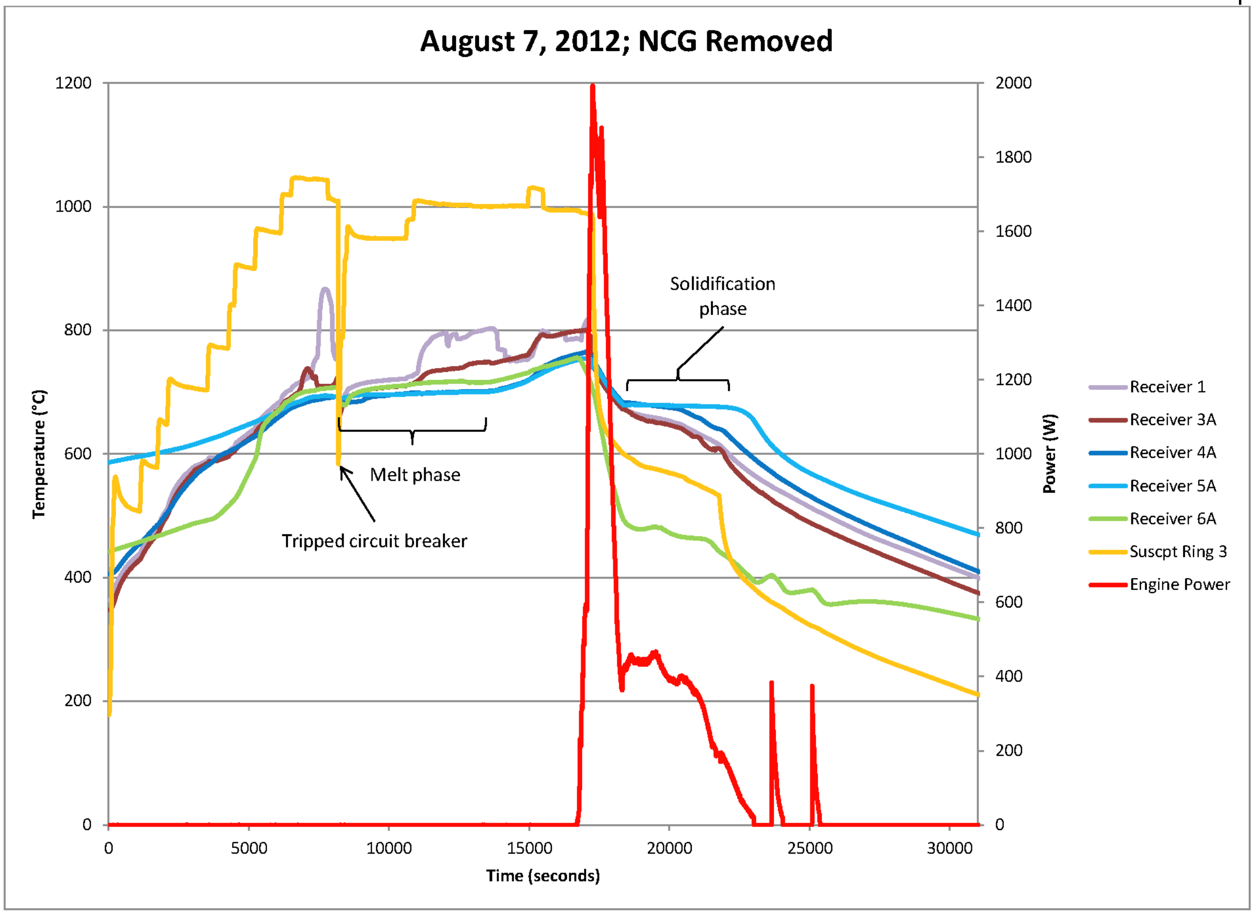

Figure 28, Modified Phase II Test Results, 7 August 2012

Again, the results did not meet expectations. Infinia arranged a meeting with heat pipe experts Thermacore to discuss the poor performance. The data seem to indicate that the problem with the heat pipe(s) in charging mode could be insufficient liquid sodium return to the evaporator; while poor discharge performance suggests salt solidification around the secondary heat pipes, impairing heat transfer due to the salt's low conductivity to a greater degree than anticipated.

One diagnostic tool according to Thermacore is to test the TES module in a horizontal orientation. All testing to date has occurred in the vertical orientation – which is also the mid-day sun position on a concentrator. This orientation is adverse to sodium condensate returning to the evaporator, as the sodium must be pumped by capillary forces against gravity to the heater head HPVC, and then travel back down the central heat pipe. Although the project end date had passed, Infinia chose to convert the test stand to a horizontal orientation in order to try to understand why the performance was lower than expected.

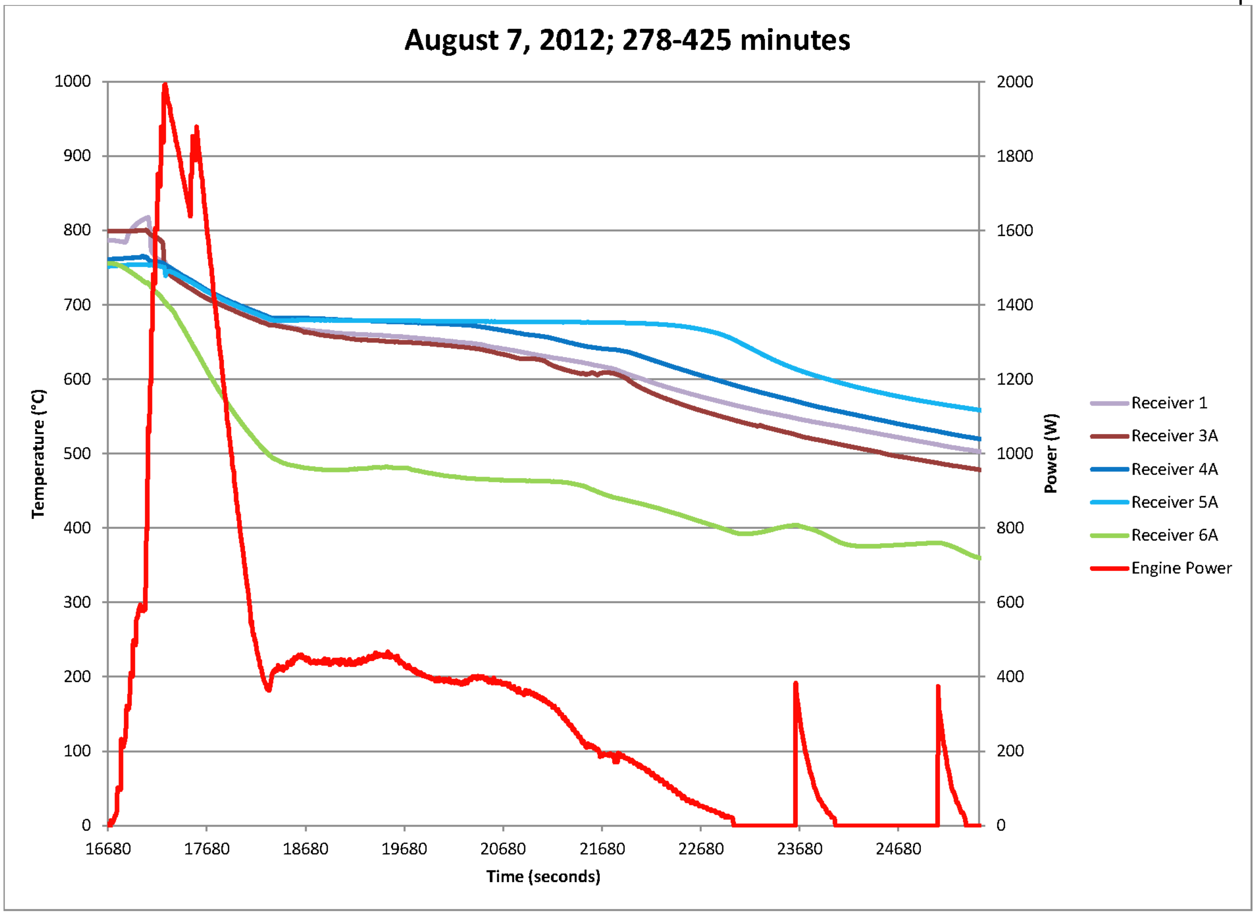

Figure 29, Test Results, 7 August 2012; 278-425 Minutes

The horizontal test was conducted October 12, 2012. Prior to the test, the engine was evacuated, and the three tape heaters energized to pre-heat the TES module to 200°C overnight. The results are shown in the plots in Figure 30 and Figure 31.

The tape heaters were turned off at the start of testing such that the sole heat input was the susceptor. The susceptor power was stepped up gradually, keeping the temperature difference between axial locations 3 and 4 no greater than 100°C. When the receiver temperature reached about 550°C, the heater head vapor chamber temperature began to rise sharply in response to the heat pipe becoming active. The heat pipe space as indicated by the temperatures at locations 1, 3 and 6 became mostly isothermal, as the salt continued to heat up and melt over the next 5 hours or so.

The TES was heated to a temperature of about 750°C, corresponding to a liquid superheated state for the salt mass. The ability of the receiver to accept heat in the horizontal orientation was significantly higher; the susceptor was generating an estimated 5.7 kW at a skin temperature of 800°C, as compared to around 3 kW during previous tests. In addition, it is evident that the secondary array of heat pipes is more effective at transferring heat, since the external heaters were not needed to help melt the salt. At just after 390 minutes, the engine was charged incrementally with helium to its full operating pressure, and the susceptor was turned off such that the engine extracts heat from the TES alone.

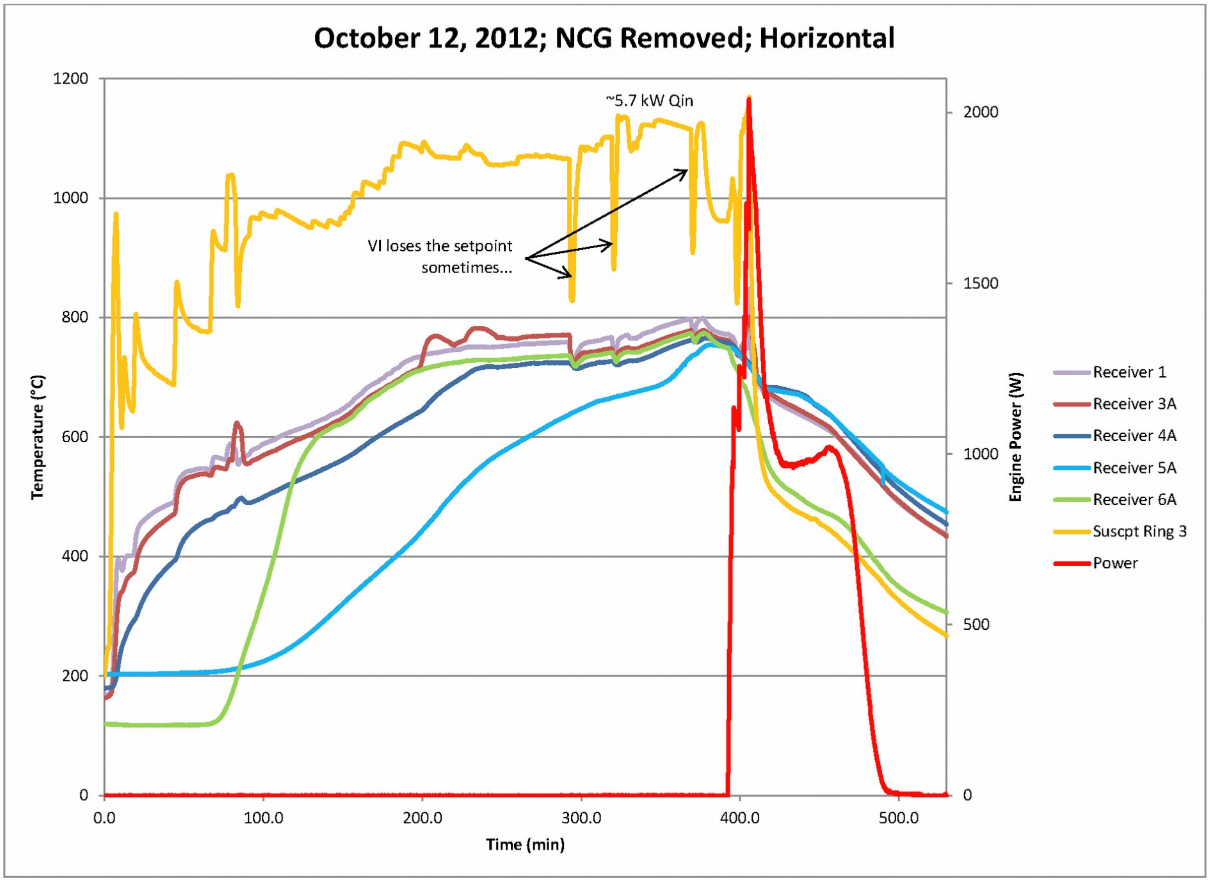

Figure 30, Horizontal Test Results, 12 October 2012

The engine power initially spiked to just over 2 kW, but then dropped rapidly as before indicating a problem with the heat pipe performance. In this case, the power level stabilized at around 1 kW as the salt solidified, as compared to 400 W when the TES was oriented vertically. This can be seen in the plot of Figure 31. The total electrical energy generated was about 1.3 kW-h until the engine stopped. This was an improvement of 400 W-h over the previous test, but still short of the goal of 3 kW-h.

This test indicates that the ability of the heat pipe wick to return sodium condensate to the receiver is inadequate in current design when the TES module is in its gravity-adverse (vertical) orientation. In both the vertical and horizontal cases, the heat pipe network is performance limited, it is very likely due the inadequate wick design or wick defects in the current TES heat pipe systems. It is encouraging however, that the engine power output is relatively constant during the salt solidification phase. This implies that the heat pipes are able to extract heat energy from the salt effectively throughout the solidification, even though the solid salt's thermal conductivity is low.

Given the shortcomings of the TES module performance, on-sun testing was not pursued.

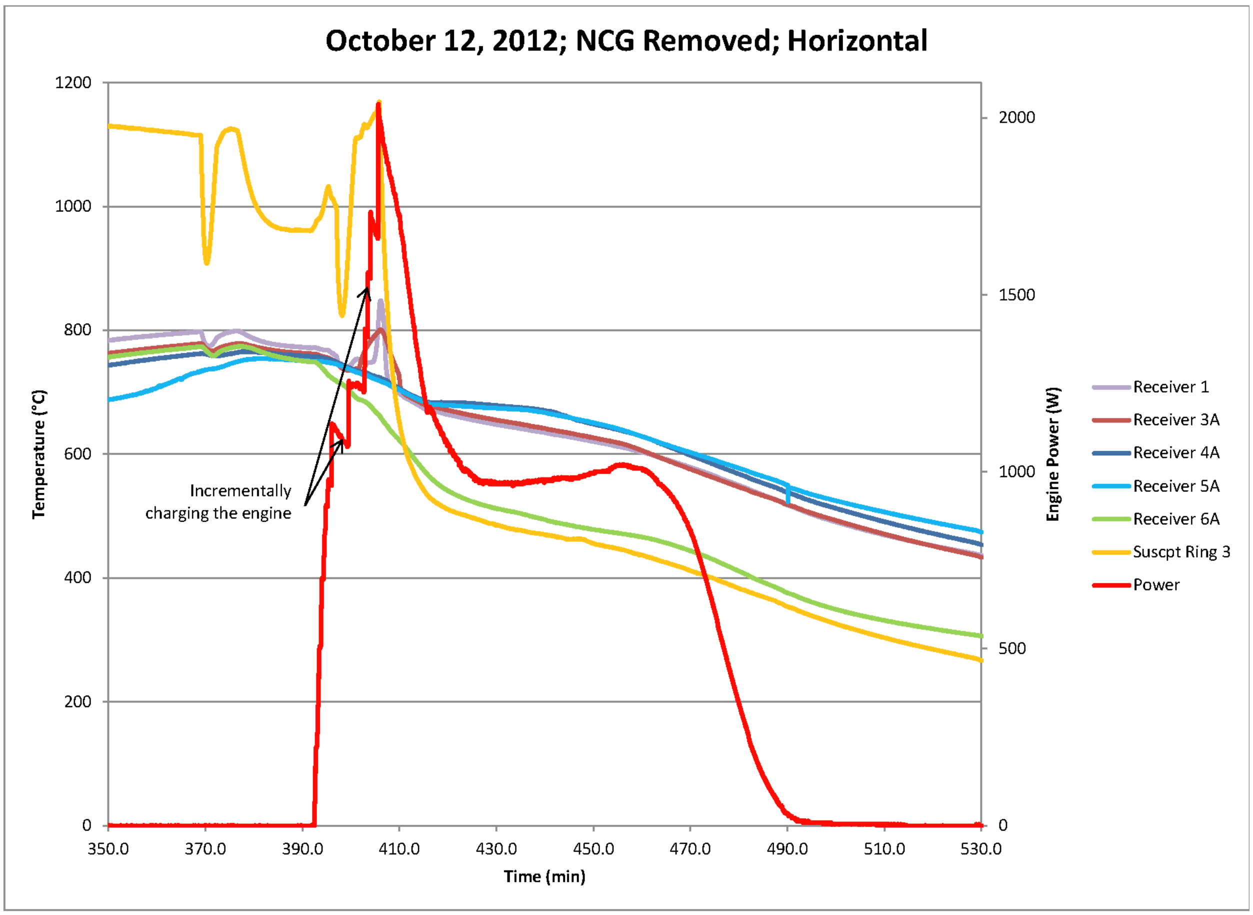

Figure 31, Test Results, 12 October 2012; 350-530 Minutes

Task 7: LCOE Refinement

This task conducts a manufacturing cost analysis and assesses the impact of the proposed TES on the LCOE of a 3-kW dish/Stirling CSP system. The cost analysis required a two-part approach. The first part entails costing the individual components that make up the TES module. Infinia contracted with automotive design and consulting firm Ricardo to provide a detailed cost analysis of these components. The second part requires an analysis of the assembly of the TES module including wick fabrication and installation, joining of the module sub-assemblies, processing the heat pipes, and filling and sealing the salt vessel. This portion of the analysis was conducted by Thermacore. A discussion of the two efforts follows.

Ricardo provided Infinia with a detailed part level cost and for sub-assemblies where appropriate, excluding capital equipment using a mixture of the following:

- Internally developed proprietary product costing models
- Boothroyd Dewhurst DFMA cost estimation software
- Subject matter expertise

Ricardo’s estimated part cost less vendor profit per unit is **$1,483.**

Thermacore’s report documented an initial review of capital, labor, and material costs for the high volume production of the TES module itself.

For large scale volume production, 40,000 TES units per year, a dedicated plant with specialized equipment is warranted. In particular vacuum furnaces are employed for several steps in the process. A total of 22 large vacuum furnaces would be required, and form the largest category of capital expense for the plant. The current design of the TES specifies several special alloys, Inconel 625 and Haynes 230. The target TES volume would make for the largest single demand in the marketplace for these alloys, and so the market price is uncertain. The salt, a blend of sodium chloride and sodium fluoride, is inexpensive as a basic commodity, but in order to suppress corrosion, high purity requirements are required. While that actual purity requirement has not been fully researched, a new supply chain will have to be developed to supply these ultra-pure salts in high volume. Consequently there is again significant uncertainty in their cost. The labor content is fairly modest. Electricity cost and shipping cost will be significant. Because those are highly location specific, the plant should be placed near the Stirling engine plant and/or in a low energy cost location.

A fabrication plan was developed to fully describe the manufacturing plant, labor, and consumables requirements. This plan is based on the fabrication steps used for the single prototype TES that has been built. Modest numbers of sodium and other high temperature heat pipes have been built by Thermacore over the last two decades, on the order of 10-50 per year. The techniques for preparing and processing the heat pipe have been found to be suitable for low volume production but have never been projected to high volume production. This LCOE study is an important first step in the path towards the volume production of high temperature heat pipes. The techniques for preparing and processing the salt canister have less grounding in experience. Because purity, especially the absence of water and oxides, are known to be important for sodium heat pipe performance and are thought to be important for corrosion-free operation of the molten salt canister, similar techniques have been proposed for the salt-side preparation and processing.

Two core steps are essential to this plan. Hermetic welding (or brazing) of the components is required to seal the sodium and salt in, and environmental gases out. This step is especially critical for this design because of the many joints; there are 82 distinct welds with an overall length of more than 5m.

The second core step is to do a vacuum bake-out of the heat pipe, and probably the salt canister as well. This involves heating the welded assembly up to a temperature above the operating temperature of the device, >750°C, while pulling a vacuum of lower than 1x10-5 Pa. This serves to remove adsorbed moisture and oxides from the surface of the heat pipe and salt canister and to allow hydrogen impregnated in the metal during forging to diffuse out of the metal.

An important follow-up step to the welding and vacuum bake-out steps is to leak check the assembly, both the heat pipe side and the salt side, with a helium mass spectrometer leak checker. The final leak rate must be less than 1x10-8 scc/sec of helium.

The area requirements and work flow arrangement of the proposed manufacturing plant are dominated by the many large vacuum furnaces. These furnaces also require support utilities such as cooling towers, nitrogen gas lines, etc. To facilitate these utilities the proposed layout of the facility is a long narrow form factor, with the vacuum furnaces and their utilities along one side. The office space, QC functions, and inventory storage are lined up along the other side. Robotic and manual welding stations are interspersed as appropriate between the various stages of vacuum furnaces.

At the rate of 159 units per day, considerable storage space and shipping traffic is required. The incoming storage and finished inventory space modeled assumes 1 week shipment intervals, by railcar. Other models are possible, such as trucking, with trailers utilized as the storage facility, or just-in-time deliveries to an adjacent facility that would incorporate the TES into the solar concentrator & Stirling engine assembly.

The staffing requirements to support a production rate of 40,000 TES units per year assume a 3- shift, 5 days per week production schedule. A rate of 0.407 days of labor per TES (about 3.5 hours each) has been tallied by the labor required to staff each of the pieces of production equipment.

The major utility costs are electrical power, water, and nitrogen. Because these utility costs are highly variable by geography, the costs for the actual site location should be adjusted accordingly.

The major cost driver for the TES is the raw material cost. With this result it is clear that major effort needs to be given to predicting the raw material costs more accurately, and to reducing those costs through redesign for manufacturing and selection of lower cost materials. The materials chosen for the prototype, Inconel 625 and Haynes 230, were specifically chosen for their corrosion resistance and compatibility with the salt and the sodium. They are among the most corrosion resistant alloys on the market, and also among the most costly. No doubt less expensive options can be developed, given sufficient effort. That effort should be focused on establishing the ability of the salt-facing materials to endure the extremely corrosive environment of molten salt.

The capital requirements are dominated by the vacuum furnaces and their associated equipment. The main function of the furnaces is to achieve the required purity levels for the hardware and salt charge, particularly to remove moisture, a key step in controlling corrosion. Just as material costs are driven by corrosion issues, so are capital costs.

High raw material costs also impact capital requirements. Raw material and finished goods inventory rival the furnace costs.

Once the costing tasks have been completed, the LCOE analysis can be conducted. The first step is to take the costing information supplied by Ricardo and Thermacore, and use it to develop a refined model for a 4-hour storage variant. Costs for the 4-hour dish as supplied by SBP are added to the model. Infinia then uses a spreadsheet model to calculate LCOE using the same methods as NREL's SAM. Energy production is calculated using a TRNSYS model developed especially for Infinia's PowerDish™ system, modified to include the thermal energy storage component. A work flow diagram of the process is given in Figure 32.

The resulting TES module cost is scaled to a four-hour variant using the following assumptions:

- Current Infinia solar engine nominal output is 3.5 kW instead of 3.0 kW; required salt volume is then scaled accordingly.
- To minimize temperature drops from the salt mass to the engine, heat pipe spacing must be arranged such that salt thickness does not exceed about 2 inches; secondary heat pipe spacing and quantities are adjusted accordingly.
- Since the heat pipe capillary pumping height limit has essentially been reached in the one-hour design, in order to increase volume, the diameter of the vessel must be scaled to increase cross-sectional area and volume.

Each component is evaluated individually for application of an appropriate scaling factor, and the resultant cost summation for a four-hour module is evaluated in the LCOE model.

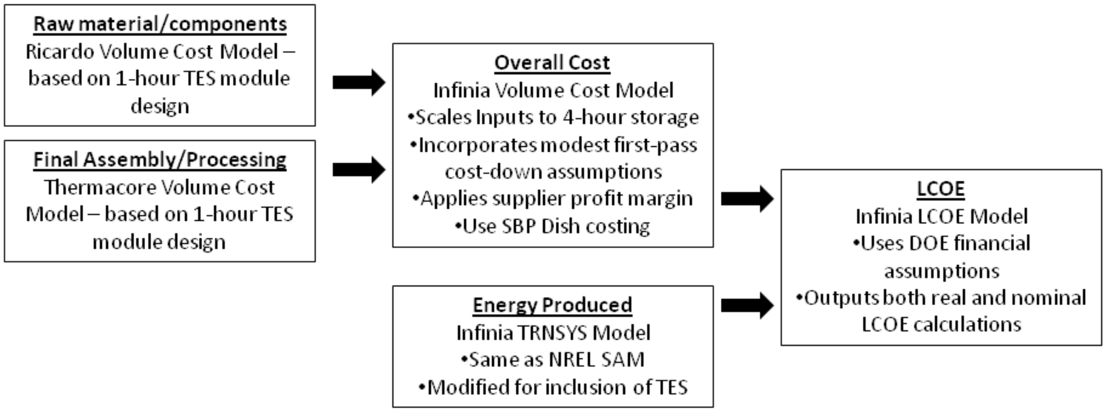

Figure 32, LCOE Evaluation Work Flow

It should also be noted that in the Infinia TES module costing model, manufacturer margin mark-ups of 20% are included, as this was not in Ricardo's estimates.

The resulting real LCOE for the Dish/Engine/TES system designed for 4-hours of energy storage is 16.19¢/kW-h. Although this is higher than current DOE goals, opportunity for improvement exists.

Conclusions:

Basic functionality of the TES system was successfully demonstrated in the laboratory, although its performance fell short of targeted nominal power output and energy production due to heat pipe system design or manufacturing defects. The real LCOE calculated for this hardware exceeded DOE goals significantly; however there are ways to further reduce the system LCOE to get close to DOE targets. Nevertheless, valuable data was obtained and many important lessons learned. With further testing and development, particularly in the area of complex liquid metal heat pipe networks, the project team feels that the technical issues can be solved. However, given the factor that the project objective for phase 3 is to design and test on sun the field ready systems while the prototype heat pipe design in the current prototype TES system requires further refinement and test demonstration, the continuation to Phase 3 is not feasible at this moment.

Budget and Schedule:

Table 1 below summarizes the project financial metrics at the end of the period of performance. A total of $38,320 was left unspent from both the DOE and Infinia cost share. This reflects the fact that on-sun testing activities were not conducted.

Table 1, Project Financial Metrics

Budget Period	Period Start Date	Government Budget	Cost Share Budget	Total Budget	Government Spent	Cost Share Spent	Total Spent	Total Remaining
1*	9/30/2008	$499,987	$124,996	$624,983	$499,986	$124,997	$624,983	$0
2	11/1/2009	$1,478,939	$369,735	$1,848,674	$1,448,284	$362,070	$1,810,354	$38,320
3	TBD	$3,443,802	$3,443,803	$6,887,605	$0	$0	$0	$6,887,605

Table 2 below summarizes the Phase 2 project Task completion dates and modifications. The project was extended twice from its original end date of November 2010. The first was the result of extensive delays in fabrication of the TES module. The second resulted from the failure experienced in the summer of 2011. Tasks 4 and 5 were inserted into the SOPO as a result of this second extension as well.

Table 2, Project Schedule

Task	Original date	Revised date
Task 1 - Detailed Integrated Design	Feb '10	Jun '10
Task 2 - Fabricate, Integrate TES/CSP Prototype	May '10	Jun '11
Task 3 - Increased Dish Capacity Design	Oct '10	Aug '11
Task 4* - Evaluate TES Module Repair	-	Feb '12
Task 5* - Repair TES Module	-	Apr '12
Task 6 – Test & Evaluate TES/CSP System Prototype	Nov '10	Aug '12
Task 7 – LCOE Refinement	Sep '10	Aug '12
Task 8 - Project Management and Reporting	Nov '10	Aug '12

References:

[1] "NREL Trough Net," 28 January 2010. [Online]. Available: http://www.nrel.gov/csp/troughnet/thermal_energy_storage.html.

[2] A. Maccari, "Innovative Heat Transfer Concepts in Concentrating Solar Fields," in *Concentrating Solar Power, Towards the 7th European RTD Framework Programme*, Brussels, 2006.

[3] J. H. e. a. Rosenfeld, "An Overview of Long Duration Sodium Heat Pipe Tests," in *Proceedings STAIF*, Albuquerque, 2004.